

Interlaboratory Comparison of Hydrogen–Deuterium Exchange Mass Spectrometry Measurements of the Fab Fragment of NISTmAb

Jeffrey W. Hudgens,^{*,†,‡,§,||} Elyssia S. Gallagher,^{†,‡,§,||} Ioannis Karageorgos,^{†,‡,§,||} Kyle W. Anderson,^{†,‡,§,||} James J. Filliben,[§] Richard Y.-C. Huang,^{||} Guodong Chen,^{||} George M. Bou-Assaf,^{||} Alfonso Espada,[#] Michael J. Chalmers,^{||} Eduardo Harguindey,[#] Hui-Min Zhang,^{||} Benjamin T. Walters,^{||} Jennifer Zhang,^{||} John Venable,^{||} Caitlin Steckler,^{||} Inhee Park,^{||} Ansgar Brock,^{||} Xiaojun Lu,^{||} Ratnesh Pandey,^{||} Arun Chandramohan,^{||} Ganesh Srinivasan Anand,^{||} Sasidhar N. Nirudodhi,^{||} Justin B. Sperry,^{||} Jason C. Rouse,^{||} James A. Carroll,^{||} Kasper D. Rand,^{||} Ulrike Leurs,^{||} David D. Weis,^{||} Mohammed A. Al-Naqshabandi,^{||} Tyler S. Hageman,^{||} Daniel Deredge,^{||} Patrick L. Wintrobe,^{||} Malvina Papanastasiou,^{||} John D. Lambris,^{||} Sheng Li,^{||} and Sarah Urata^{||}

[†]Bioprocess Measurement Group, Biomolecular Measurements Division, National Institute of Standards and Technology, Rockville, Maryland 20850, United States

[‡]Institute for Bioscience and Biotechnology Research, 9600 Gudelsky Drive, Rockville, Maryland 20850, United States

[§]Statistical Engineering Division, National Institute of Standards and Technology, Gaithersburg, Maryland 20899, United States

^{||}Pharmaceutical Candidate Optimization, Research and Development, Bristol-Myers Squibb Company, Princeton, New Jersey 08540, United States

[⊥]Analytical Development, Biogen Inc., 225 Binney Street, Cambridge, Massachusetts 02142, United States

[#]Centro de Investigación Lilly S.A., 28108 Alcobendas, Spain

[∇]Lilly Research Laboratories, Eli Lilly and Company, Indianapolis, Indiana 46285, United States

[○]Protein Analytical Chemistry, Genentech, Inc., 1 DNA Way, South San Francisco, California 94080, United States

[◆]Genomics Institute of the Novartis Research Foundation, 10675 John Jay Hopkins Drive, San Diego, California 92121, United States

[¶]Joint Center for Structural Genomics, La Jolla, California 92037, United States

[□]MedImmune LLC, One MedImmune Way, Gaithersburg, Maryland 20878, United States

[⊗]Department of Biological Sciences, National University of Singapore, 14, Science Drive 4, Singapore 117543

[■]Vaccine R&D, Pfizer Inc., 401 N Middletown Rd, Pearl River, New York 10965, United States

[△]Analytical R&D, Pfizer Inc., 700 Chesterfield Parkway West, Chesterfield, Missouri 63017, United States

[●]Analytical R&D, Pfizer Inc., 1 Burt Road, Andover, Massachusetts 01810, United States

[±]Department of Pharmacy, University of Copenhagen, Universitetsparken 2, DK-2100 Copenhagen, Denmark

[▲]Department of Chemistry, University of Kansas, 1567 Irving Hill Road, Lawrence, Kansas 66045, United States

[◇]Department of General Science, Soran University, Kawa Street, Soran, Kurdistan Region, Iraq

[★]Department of Pharmaceutical Sciences, University of Maryland, Baltimore, School of Pharmacy, 20 North Pine Street, Baltimore, Maryland 21201, United States

[◁]Department of Pathology & Laboratory Medicine, Perelman School of Medicine, 402 Stellar-Chance Laboratories, University of Pennsylvania, 422 Curie Boulevard, Philadelphia, Pennsylvania 19104, United States

[▷]Department of Medicine, University of California, San Diego, 9500 Gilman Drive, La Jolla, California 92093, United States

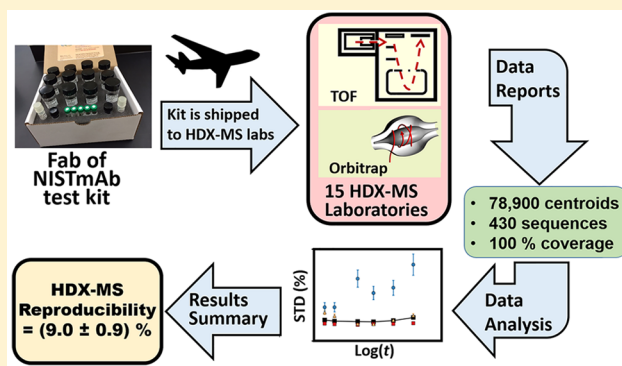
S Supporting Information

Received: March 1, 2019

Accepted: May 2, 2019

Published: May 2, 2019

ABSTRACT: Hydrogen–deuterium exchange mass spectrometry (HDX-MS) is an established, powerful tool for investigating protein–ligand interactions, protein folding, and protein dynamics. However, HDX-MS is still an emergent tool for quality control of biopharmaceuticals and for establishing dynamic similarity between a biosimilar and an innovator therapeutic. Because industry will conduct quality control and similarity measurements over a product lifetime and in multiple locations, an understanding of HDX-MS reproducibility is critical. To determine the reproducibility of continuous-labeling, bottom-up HDX-MS measurements, the present interlaboratory comparison project evaluated deuterium uptake data from the Fab fragment of NISTmAb reference material (PDB: 5K8A) from 15 laboratories. Laboratories reported $\sim 89\,800$ centroid measurements for 430 proteolytic peptide sequences of the Fab fragment ($\sim 78\,900$ centroids), giving $\sim 100\%$ coverage, and $\sim 10\,900$ centroid measurements for 77 peptide sequences of the Fc fragment. Nearly half of peptide sequences are unique to the reporting laboratory, and only two sequences are reported by all laboratories. The majority of the laboratories (87%) exhibited centroid mass laboratory repeatability precisions of $\langle s^{\text{Lab}} \rangle \leq (0.15 \pm 0.01) \text{ Da}$ ($1\sigma_x$). All laboratories achieved $\langle s^{\text{Lab}} \rangle \leq 0.4 \text{ Da}$. For immersions of protein at $T_{\text{HDX}} = (3.6 \text{ to } 25)^\circ\text{C}$ and for D_2O exchange times of $t_{\text{HDX}} = (30 \text{ s to } 4 \text{ h})$ the reproducibility of back-exchange corrected, deuterium uptake measurements for the 15 laboratories is $\sigma_{\text{reproducibility}}^{15 \text{ Laboratories}}(t_{\text{HDX}}) = (9.0 \pm 0.9) \%$ (1σ). A nine laboratory cohort that immersed samples at $T_{\text{HDX}} = 25^\circ\text{C}$ exhibited reproducibility of $\sigma_{\text{reproducibility}}^{25^\circ\text{C cohort}}(t_{\text{HDX}}) = (6.5 \pm 0.6) \%$ for back-exchange corrected, deuterium uptake measurements.



INTRODUCTION

Over the last 28 years hydrogen–deuterium exchange mass spectrometry (HDX-MS) has developed into a powerful tool for investigating conformations, folding dynamics, and interactions among proteins including antibodies, glycoproteins, lipoproteins, membrane proteins, virus fragments, enzymes, chaperones, amyloids, fibrils, and pharmaceuticals.¹ The steady growth of HDX-MS studies is reflected in the 2247 original, heavily cited research publications appearing through 2018 (Figure S1).² In the commercial sector HDX-MS data has been used to substantiate and protect intellectual property in more than 110 United States patents since 2010.³ HDX-MS data are increasingly provided to support biologics license applications (BLAs).⁴ During 2016, 15% of BLAs to the Food and Drug Administration (FDA) included HDX-MS data.⁵ The increasing use of HDX-MS has been facilitated by rapid advances in the hardware and software that collect and analyze HDX-MS kinetics measurements. In short, HDX-MS has emerged from the “quicksand” of frontier science,⁶ and it has become a mainstay tool in modern pharmaceutical^{4,7–26} and structural biology laboratories.^{3,23,27–35}

Major advantages of HDX-MS for characterizing the conformational dynamics of proteins are its availability to make measurements under physiological conditions, its modest sample requirements, its use of proteomic informatics that link each HDX-MS peptide sequence directly to a portion of the subject protein, and its nearly unlimited capability to characterize large proteins, for example, antibodies ($\sim 150 \text{ kDa}$)^{10,12,16,19,35} and viral capsids ($\sim 2 \text{ MDa}$).^{36–42} The spatial structure obtained from X-ray and NMR structure analyses, cryogenic electron microscopy (cryo-EM), and the molecular dynamics revealed by HDX data can provide an improved description of the structure–function–dynamics relationships of a protein.⁴³

HDX-MS is projected to have a role in quality control of biopharmaceuticals and for establishing dynamic similarity between a biosimilar and an innovator drug.^{7,10,22,44,45} As HDX-MS measurements are used to characterize materials that

will enter commerce, customers may ask: How true and precise is the HDX-MS measurement?

Trueness is the nearness of agreement between the average of a large number of replicate measurements and a reference value.^{46,47} Although numerous approaches to the prediction of H/D exchange rates coefficient are reported,^{48–54} no means of accurately predicting exchange rates from first-principles currently exist, and no reference materials with known exchange rates are available. Thus, on the one hand, we cannot easily establish the trueness of HDX-MS measurements. On the other hand, the precision metrics of HDX-MS can be evaluated, because precision is just the closeness of agreement among measured values obtained by replicate measurements on the same or similar objects under specified conditions.⁴⁶ Precision is characterized by the components of repeatability, intermediate measurement precision (IMP), and reproducibility.⁴⁶ Determinations of reproducibility allow for variations of instruments, reagents, locations, and operators.

HDX-MS studies have reported daily repeatability ranging between 0.3% and 2.9% of maximum deuterium uptake and IMP's ranging between 1% and 9% over periods of 37 d to eight months.^{7,55–58} Cummins et al. compared HDX-MS measurements for two laboratories harmonized by employing identical procedures and equipment. For ligand-vitamin D nuclear receptor complexes immersed for 30 s in D_2O their results exhibited D-uptake repeatability and reproducibility of 0.54% for a set of 35 peptide sequences.⁵⁹

The objective of this study is to determine the reproducibility of continuous-labeling, bottom-up HDX-MS measurements (Figure 1).⁶⁰ Reproducibility is determined only through an interlaboratory comparison exercise that engages multiple laboratories in measurements of the same sample.⁴⁶ For the present unharmonized study investigators were permitted use of any HDX-MS instrumentation and software. The laboratories were not directed to report specific peptide sequences, nor were they told the deuterium uptake rates of previously observed peptides. A determination of HDX-MS reproducibility will provide a measure of its present capability for evaluations of protein commercial products. Furthermore, an interlaboratory

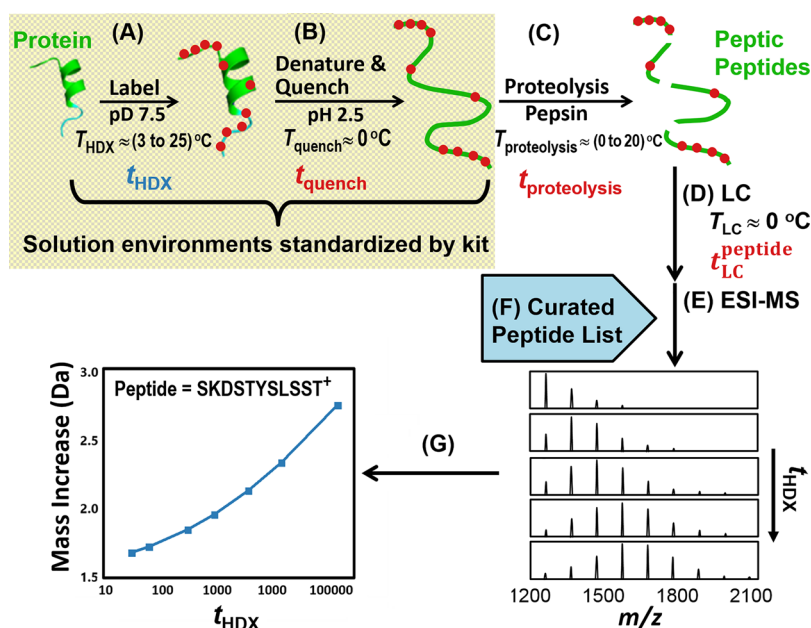


Figure 1. Bottom-up HDX-MS experiment broken into steps controlled by the NIST HDX-MS reagent kit (steps A and B in the yellow/gray box) and by each participating laboratory peptide (steps C through G). H for D back-exchange occurs during periods listed in red.

comparison project can itself stimulate improvements in measurement procedures and equipment.

EXPERIMENTAL METHODS

Bottom-up HDX-MS Measurements. Laboratories conducted “bottom-up” HDX-MS experiments (Figure 1), using procedures known to provide excellent repeatability precision.^{60–63} Immersion of Fab fragment of NISTmAb reference material (PDB: 5K8A)^{64–66} sample in buffered solution (deuterium fraction, $F^{\text{D}_2\text{O}} = 0.8$ to 0.96) at temperature T_{HDX} and pH 7.48 induces D for H exchange (Figure 1A). At t_{HDX} the solution is diluted into an acidic solution ($T_{\text{quench}} \approx 0^\circ\text{C}$, pH ≈ 2.5 , $F^{\text{D}_2\text{O}} = 0.18$ to 0.48), containing chaotropic and reducing agents,⁶⁷ which denature the protein and reduce its disulfide bonds (Figure 1B). In this cold acidic solution, chemical exchange rates of amide sites in denatured proteins approach their minima.⁶⁸ All laboratories used the same HDX-MS kit (Figure S2) that provided buffers and reagents used during the first two steps (ref yellow/gray box of Figure 1). The kit harmonized pH, salt concentration, and reducing power (Table S1). However, specific requirements of laboratory apparatus (Tables S2–S4) required adjustments to protein concentrations and $F^{\text{D}_2\text{O}}$ (Table S5).

Subsequently, the denatured, quenched Fab solution passes into a column containing immobilized pepsin or pepsin/protease from *Aspergillus saitoi* type XIII blend (Figure 1C).^{25,69,70} The protease digests the Fab fragment of NISTmAb ($\Delta t_{\text{proteolysis}} = (18 \text{ to } 240) \text{ s}$, $T_{\text{proteolysis}} = (0 \text{ to } 20)^\circ\text{C}$), and the peptides within the effluent become trapped on a guard column (Figure 1D). By flowing additional solution through the guard column for $t_{\text{wash}} = (30 \text{ to } 180) \text{ s}$, many laboratories wash out salts. Reverse-phase chromatography, conducted at $T_{\text{LC}} \approx 0^\circ\text{C}$, releases and separates peptides, which elute from the analytical column at $t_{\text{LC}}^{\text{peptide}}$ (Figure 1D). Electrospray ionization mass spectrometry (ESI-MS) detects the peptide ions (Figure 1E).

Alternately, immediately after D_2O incubation has completed (Figure 1B), some laboratories flash freeze the sample (Table

S5). Subsequently, the sample is thawed and analyzed using a workflow similar to that depicted in Figures 2C–G.

The average mass change of each selected peptide (Figure 1F) is calculated and plotted as a function of t_{HDX} (Figure 1G). Since side-chain amides generally exchange H/D more rapidly than backbone amides,^{62,68} the deuterium labels at these positions will have equilibrated during chromatography to the natural protic isotope abundance, thus, simplifying analyses.

Separate experiments, equivalent to the HDX-MS experiment for $t_{\text{HDX}} = 0 \text{ s}$, determine the initial curated list of peptides (Figure 1F) that associates each chromatographic peak with mass spectra. To improve the veracity of peptide identifications, the operator observes MS/MS data for the eluting peptides. With reference to the known sequence of Fab of NISTmAb⁶⁵ peptide ion identification software (Tables S2 and S3) analyzes these data and proposes an amino acid sequence, charge state (z), and confidence rank for each peptide ion fragment. The list of retention times and sequences becomes the filter through which peptide ions are selected for HDX-MS analyses. Still, the curation process continues throughout the data analysis. Curation of the list ascertains that the exchange kinetics of sequences adhere to EX2 behavior,^{1,71–73} that the D-uptake kinetics match the sequence assignments, that the LC retention times remain stable, and that peptides exhibit adequate intensity to support reliable centroid determinations and remain free of interfering ion signals.

Each laboratory conducted proteomics studies on the Fab fragment of NISTmAb and performed three HDX-MS runs. Each “run” comprises three replicant measurements, termed “reps”, at each time point, t_{HDX} . Laboratories submitted spreadsheets of centroids and information about experimental conditions to a not-for-profit data service, National Association for Proficiency Testing (NAPT), Edina, MN, which anonymized the datasheets and forwarded them to the National Institute of Standards and Technology (NIST). The data are available for study.⁷⁴

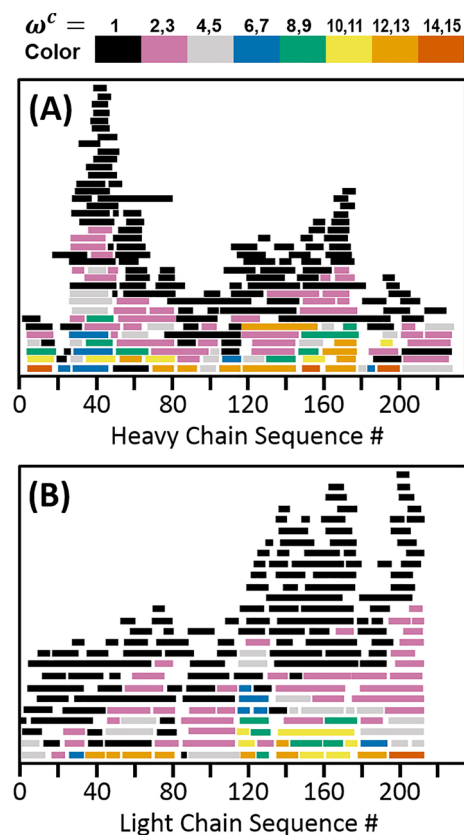


Figure 2. Reference peptide heat map of the peptide sequences reported by 15 laboratories for Fab fragment of NISTmAb. Colors indicated on the legend denote the ω_i^c of each peptide sequence. Vertical placements of the sequence stripes are determined by sequence overlap and ω_i^c . Horizontal placements of stripes denote peptides between the N-terminal and C-terminal sequence indices for the (A) 221 sequences reported for the heavy chain and (B) 209 sequences reported for the light chain.

RESULTS

Laboratory Reports. The NIST Interlaboratory Comparison Project received 15 anonymized data sets and associated documentation. The 15 data sets contain $\sim 89\,800$ HDX-MS centroid measurements from 709 peptide ions, ranging from 456 to 6048 m/z and $1 \leq z \leq 8$, comprising 507 unique amino acid sequences.

A few laboratories reported sequences of the Fc fraction of NISTmAb. These sequences were expected due to trace Fc present in the Fab stock solution. Since most of the laboratory cohort did not report Fc peptides, 100 Fc peptide ions (77 Fc sequences) were deleted from the working data set. The reduced working data set for the Fab protein comprises $\sim 78\,900$ centroids. The working data set contains 609 peptide ions originating from 430 sequences of the light and heavy chains.

Laboratories reported the centroid mass ($m(t_{\text{HDX}})$), derived for each measurement at seven D_2O immersion times (Figure 1A), $t_{\text{HDX}} = 0, 30, 60, 300, 900, 3600$, and $14\,400$ s. By measuring peptide ions observed from the finished Fab- D_2O sample, laboratories computed the centroid mass control value, $\langle m(\infty_{\text{pseudo}}) \rangle$, corresponding to $t_{\text{HDX}} \approx \infty$ s.

Reference Peptide Maps. Colored stripes, Figure 2, illustrate the peptide ion sequences reported by all laboratories. With reference to the legend of Figure 2, the color of each stripe indicates its coincidence frequency (ω_i^c), which is the number of

laboratories reporting the i th peptide sequence (ion of any z). The x -coordinates of each stripe correspond to the start and stop indices of the peptide sequence with reference to the Fab fragment of NISTmAb. The y -coordinate position of each strip allows a unique address for each sequence. The software drawing this map places the most frequently reported sequences (largest ω_i^c) at the lower ordinates. Where peptides of the same ω_i^c would overlap, one peptide is placed in the next higher vertical row.

Summation of all data for the Fab fragment yields a map of the heavy chain containing 221 peptide sequences (Figure 2A) and a map of the light chain containing 209 peptide sequences (Figure 2B). The sequences comprise between 4 and 60 amino acids. The set of 430 sequences reported by the laboratories has a median sequence length of 13 amino acids, and 84% of the members in the set contain between 5 and 21 amino acids (Figure S3).

Although the laboratory cohort collectively reports sequences that cover the heavy and light chains comprehensively, most laboratories reported data sets holding lower sequence coverage. The peptide sequences reported by the laboratories number between 41 and 175, corresponding to coverages from 56% to 99% for the heavy chain and from 60% to 99% for the light chain (Figure S4).

The sequence coincidence population, $M(\omega^c)$, is computed by counting the peptide sequences for each coincidence frequency, ω^c . For example, $M(1) = 245$ (represented by black stripes in Figure 2) is the population of sequences listed once across all laboratory data sets. The population $M(1)$ of the Fab fragment comprises 48% heavy-chain sequences and 53% light-chain sequences. In Figure 2 stripes of other color bars represent sequences listed twice or more across all laboratory data sets ($2 \leq \omega_i^c \leq 15$); thus, $\sum_2^{15} M(\omega^c) = 185$ shared peptide sequences. (The working data set is $\sum_1^{15} M(\omega^c) = 430$.) Across the laboratory cohort, $M(\omega^c)$ falls rapidly with increasing coincidence frequency, such that only two peptide sequences are reported by all laboratories, that is, $M(15) = 2$ (Figure S5).

The number of reported peptide sequences as a function of the six instrument-software configurations used by the laboratories was examined (Figure S6). On average, laboratories reported $\langle \bar{C} \rangle = 103 \pm 41$ (1σ) sequences. No laboratory reported peptide sequence populations falling outside the $\langle \bar{C} \rangle \pm 3\sigma$ boundaries that would identify outlying performance. This result suggests that each instrumentation-software configuration has nearly equal capacity to detect the numerous Fab fragments of NISTmAb emanating from its ESI source. Furthermore, we note that the use of a pepsin/Type XIII protease mixture by Lab 12 did not lead to identification of a superior, outlying number of peptides in comparison to the cohort using pepsin only.

Sensitivity Analyses of HDX-MS Measurements. Knowledge the overall effect of experimental factors will guide evaluation of the measurement uncertainty. One possible error could arise if the deuterium content of peptides varies as a function of charge.^{75,76} Thus, deuterium content of centroids versus peptide charge was examined for 513 peptides ($z = +1$ to $+7$) of 106 sequences reported by 13 laboratories. No evidence of systemic, in-ESI source, intermolecular H/D exchange was observed (Table S6).

Main effects plots reveal the overall effect of several experimental factors on the HDX-MS measurement.⁷⁷ The main effects of each independent variable on the $\%E_{\text{uncorrected}}$ and $\%E_{\text{corrected}}$ uptake measurements are found by averaging across the levels of the other independent variables of the HDX-MS experiment. For this study main effects are computed for the

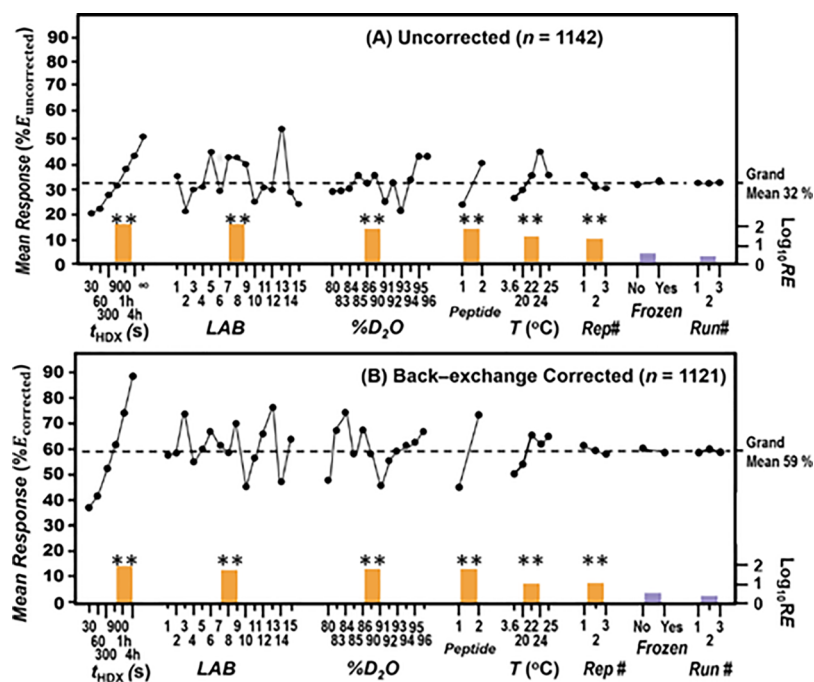


Figure 3. Main effects plots showing the variation of HDX-MS measurements for (A) data uncorrected for back-exchange and (B) data corrected for back-exchange. Bars denote $\log_{10}(\text{RE})$ for each factor. Factors found by ANOVA to exert significant relative effect ($p < 0.01$) are marked with **. Dashed lines mark the mean deuterium uptake.

factors of t_{HDX} ; *Lab*; $\%D_2O$; *Peptide*; T_{HDX} ; *Rep#*, repetition number; *FROZEN*, which is the flash-freezing of quenched sample prior to proteolysis; and *Run#*, run number. These computations used ~ 1120 measurements reported by all laboratories for the two peptides: peptide 1, $^{149}\text{VKDYF-PEPVT}^{158}$ of the heavy chain and peptide 2, $^{195}\text{VTHQG-LSSPVTKSFNRGEC}^{213}$ of the light chain.

Figure 3A displays main effects for $\%E_{\text{uncorrected}}$, which are centroids processed with equation S3 and averaged from each variable. Figure 3B displays the main effects plots for $\%E_{\text{corrected}}$, which was computed with equation S5. On each panel a dashed line marks the *grand mean* of deuterium exchange, which is the average of data from all laboratories for both peptides. (We note that the correction for back-exchange increases the *grand mean* deuteration of the two peptides from 32% to 59%.) Factors are ranked from left to right in accord with decreasing relative effect (RE). Below each plot a colored bar shows the $\log_{10}\text{RE}$, which indicates the sensitivity for each factor.⁷⁷ To assess the statistical significance of the variance within the eight factors, analysis of variance (ANOVA) computations were performed.^{77–79} In Figure 3 factors exhibiting significant relative effect ($p < 0.01$) are marked with **.

As shown in Figure 3, some factors respond in good accord with the design of the HDX-MS experiment. As examples, *mean response* ($\%E_{\text{uncorrected}}$) rises from 18% to 48% between $t_{\text{HDX}} = 30$ s and $t_{\text{HDX}} = \infty_{\text{pseudo}}$ s, and peptides 1 and 2 exhibit different mean response, as expected for sequences residing in different local structural environments. Examination of the results for the procedure where samples are flash frozen (*FROZEN* = “yes”) indicate that this procedure has little effect on precision. The *mean response* $\%E_{\text{uncorrected}}$ suggests a 1% improvement in deuterium recovery; however, *mean response* $\%E_{\text{corrected}}$ reverses this effect by -2% . Likewise, *mean response* ($\%E_{\text{uncorrected}}$) for *Run#* 1, 2, and 3 vary by less than 0.3%, which provides assurance that day-to-day system performance is nearly invariant. These

same trends are also observed in plots of $\%E_{\text{corrected}}$. ANOVA computations also confirm insignificant variances for factors *FROZEN* and *Run#*.

Main effects analyses reveal four nonideal responses, and ANOVA verifies the significance of the variances. $\%E_{\text{peptide}}^{\text{peptide}}$ should not vary with factors of *Lab* or $\%D_2O$. Figure 3 shows that the *mean response* $\%E_{\text{uncorrected}}^{\text{peptide}}$ and *mean response* $\%E_{\text{corrected}}^{\text{peptide}}$ vary significantly for both factors. Moreover, the ideal HDX-MS experiment should exhibit null main effects with respect to *Rep#*; however, the *mean response* $\Delta(\%E_{\text{uncorrected}})$ exhibits an $\sim 3.5\%$ reduction between *Rep* 1 and *Rep* 3. After back-exchange correction the mean change remains $\Delta(\%E_{\text{corrected}}) = 3.5\%$. Since each series of reps is executed within the same run, the diminished response is likely a symptom of incomplete removal of peptides from the chromatographic apparatus between the replicate measurements.^{80,81}

Temperature also affects acid- and base-catalyzed hydrogen–deuterium exchange rates. Amides undergo $\sim 3\times$ increases in exchange rates for each increment of 10°C .⁸² In accord with this prediction, *mean response* of $\%E_{\text{corrected}}$ (Figure 3B) increases as a function of T_{HDX} between 3.6 and 25°C ; however, some possible discordant response is displayed between 22 and 25°C . Since the responses at 22 and 24°C originate from two and one laboratories, respectively, it is difficult to separate effects of *Lab* and T_{HDX} . The main effects method does not reveal factors contributing to this incongruous response.

Determinations of Repeatability. Repeatability measurements provide insight into the m/z measurement stability of the sample handling, mass spectrometer, software, and procedures. Figure 4 presents the fits for $\langle s^{\text{Lab}} \rangle$ versus $\log_{10}(t_{\text{HDX}})$ for $t_{\text{HDX}} = 0$ s through $t_{\text{HDX}} = \infty_{\text{pseudo}}$ s for each laboratory. The repeatability plot for each laboratory is constructed from a data set comprising between 984 and 4057 $s_{\text{peptide}}^{\text{Lab}}(t_{\text{HDX}})$ values from 41 to 175 sequences in all reported charge states (Figure S7). Uncertainty bars on the $\langle s^{\text{Lab}} \rangle$ symbols indicate the standard

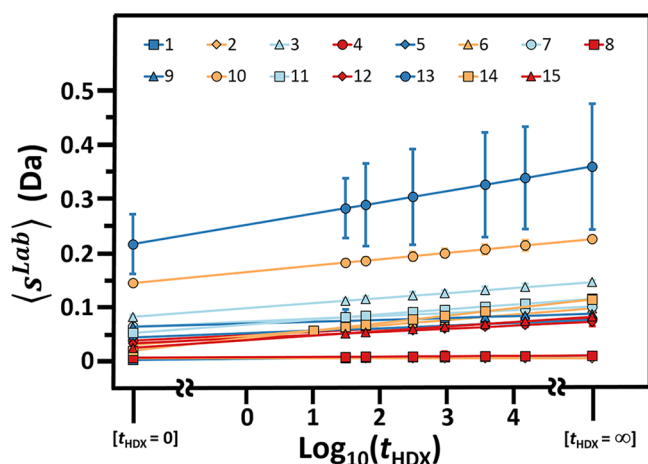


Figure 4. Repeatability plotted as average standard deviation $\langle s^{Lab} \rangle$ vs $\log_{10}(t_{HDX})$ for all peptide ions reported by each laboratory. When greater than the symbol, bars on each time point indicate one standard error of the mean, $\sigma_{\bar{x}}$.

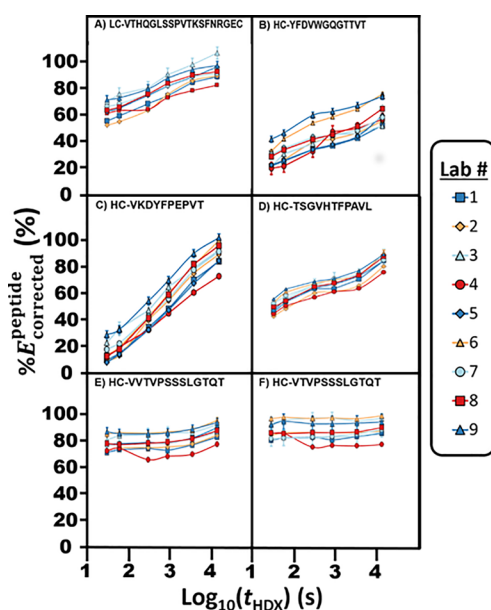


Figure 5. Plots of $\%E_{corrected}^{peptide}(t_{HDX})$ vs $\log_{10}(t_{HDX})$ for peptides measured at $T_{HDX} = (25 \pm 1)^\circ\text{C}$. (A) LC- $^{195}\text{VTHQGLSSPVTKSFNRGEC}^{213}$, (B) HC- $^{106}\text{YFDVWVGQGTITV}^{117}$, (C) HC- $^{149}\text{VKDYFPEPVT}^{158}$, (D) HC- $^{167}\text{TSGVHTFPAVL}^{177}$, (E) HC- $^{188}\text{VTVTPSSSLGTQT}^{200}$, and (F) HC- $^{189}\text{VTVTPSSSLGTQT}^{200}$. Bars denote sample standard uncertainties larger than 1%.

error of the mean, $\sigma_{\bar{x}}$. For most laboratories $\sigma_{\bar{x}} < 0.007$ Da, which corresponds to the size of the symbols in Figure 4. In summary, 87% of laboratories exhibited centroid mass laboratory repeatability precisions of $\langle s^{Lab} \rangle \leq 0.15$ Da, and the remaining 13% have repeatability precisions characterized by $0.14 \text{ Da} \leq \langle s^{Lab} \rangle \leq 0.4$ Da.

Reproducibility of HDX-MS. Reproducibility of HDX-MS is derived using sample standard deviations (equation S6) of $\%E_{corrected}^{peptide}$ for peptide sequences measured at the same T_{HDX} . The laboratories were divided into cohorts that measured $\%E_{corrected}^{peptide}$ at $T_{HDX} = (25 \pm 1)$, (21 ± 1) , and $(3.6 \pm 1)^\circ\text{C}$. Figure 5 shows plots of $\%E_{corrected}^{peptide}$ versus $\log_{10}(t_{HDX})$ that were reported by the nine laboratories of the $(25 \pm 1)^\circ\text{C}$ cohort. Figure 6A plots the

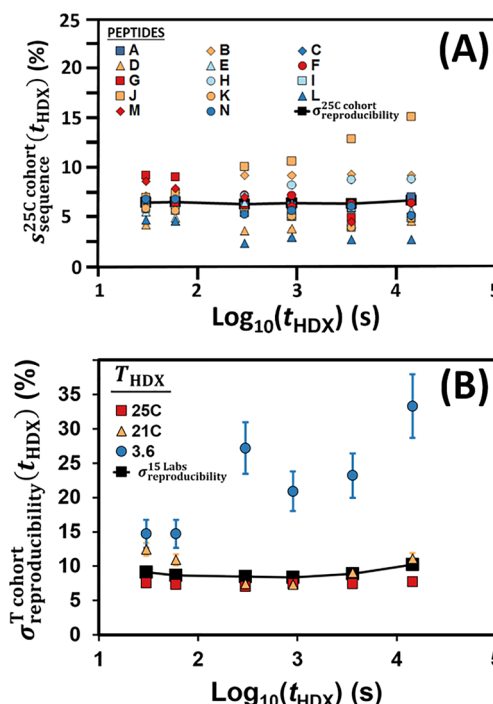


Figure 6. Determinations of HDX-MS reproducibility based on the sample standard deviation of $\%E_{corrected}^{peptide}$ for peptide sequences. (A) $\sigma_{sequence}^{25C\ cohort}(t_{HDX})$ (%) as a function of $\log_{10}(t_{HDX})$ for 14 sequences measured at $T_{HDX} = (25 \pm 1)^\circ\text{C}$. Symbols denote the data from Peptides A–G (Figure 5) and Peptides H–N (Figure S8). Black squares and a trend line denote, $\sigma_{sequence}^{25C\ cohort}(t_{HDX})$ (%) vs $\log_{10}(t_{HDX})$. Each black square is larger than the standard error of the mean, $\sigma_{\bar{x}} \approx 0.3\%$. (B) $\sigma_{reproducibility}^{T\ cohort}(t_{HDX})$ (%) vs $\log_{10}(t_{HDX})$ determined from $\%E_{corrected}^{peptide}$ for sequences measured at $T_{HDX} = (25 \pm 1)$, (21 ± 1) , and $(3.6 \pm 1)^\circ\text{C}$. Black squares and the trend line plot the weighted $\sigma_{reproducibility}^{15\ Laboratories}(t_{HDX})$ (%) vs $\log_{10}(t_{HDX})$. Each black square is larger than its standard error of the mean, $\sigma_{\bar{x}} \leq 0.9\%$.

sample standard deviations as a function of $\log_{10}(t_{HDX})$ for peptides A–F (Figure 5) and peptides G–N (Figure S8). Each plot exhibits self-consistent D-uptake patterns. Figures S8D, S8G, S8L, and S8N exhibit D-uptake traces suggestive of kinetics that may be fit with multiple-exponential functions.⁸³ The weighted arithmetic mean of these standard deviations is $\sigma_{sequence}^{25C\ cohort} = (6.5 \pm 0.6)\%$. The nearly equal weighting of data from all laboratories ($\omega_i^c = 8, 9$) gives considerable statistical significance to this result.

The determination of $\sigma_{reproducibility}^{25C\ cohort}$ is also computed by expanding this analysis to include the complete subset of 130 sequences of $\omega_i^c \geq 2$ and weighting each $\sigma_{sequence}^{25C\ cohort}(t_{HDX})$ by the number of reporting laboratories. This computation yields $\sigma_{reproducibility}^{25C\ cohort}(t_{HDX}) = (7.4 \pm 0.3)\%$. While robust, this value reflects skew from unequal weighting given by laboratories that have reported the most sequences. Reproducibility was also evaluated for $\omega_i^c \geq 2$ sequences in other temperature cohorts (Figure 6b). Table 1 summarizes the determinations of $\sigma_{reproducibility}^{cohort}$ and the associated sample standard deviations of all temperatures is $\sigma_{reproducibility}^{15\ Laboratories}(t_{HDX}) = (9.0 \pm 0.9)\%$, where the weighting factors are a product of ω_i^c and the number of sequences.

DISCUSSION

The NIST HDX-MS interlaboratory comparison project has found that 87% of the laboratory cohort achieved a measure-

Table 1. Summary of Reproducibility Determinations for Bottom-up HDX-MS for $t_{\text{HDX}} = (30 \text{ to } 14\,400) \text{ s}$

$T_{\text{HDX}}, ^\circ\text{C}$	lab cohort size	number of sequences	ω_i^c	STD ^a , %	$\sigma_{\bar{x}}^{\text{wtd}}, \%$
25 ± 1	9	14	8 to 9	6.5	0.6
25 ± 1	9	130	2 to 9	7.4	0.3
21 ± 1	4	88	2 to 4	9.7	0.7
3.6 ± 1	2	26	2	22.3	3.1
wtd mean	15	244		9.0	0.9

^a $\sigma_{\text{reproducibility}}^{\text{cohort}}$

ment repeatability precision of $\langle s^{\text{Lab}} \rangle \leq 0.15 \pm 0.01 \text{ Da}$ ($1\sigma_{\bar{x}}$). All laboratories exhibited repeatability of $\langle s^{\text{Lab}} \rangle < 0.4 \text{ Da}$. The main effects analysis and measurements on 244 shared sequences determined that the reproducibility of HDX-MS is $\sigma_{\text{reproducibility}}^{15 \text{ Laboratories}} = (9.0 \pm 0.9) \%$. Laboratories in the $(25 \pm 1) ^\circ\text{C}$ cohort realized the reproducibility $\sigma_{\text{reproducibility}}^{25^\circ\text{C cohort}} = (6.5 \pm 0.6) \%$.

This analysis used the correction for D_2O fraction and for back-exchange through measurements of $\langle m(0) \rangle^{\text{peptide}}$, $\langle m(t_{\text{HDX}}) \rangle^{\text{peptide}}$, and $\langle m(\infty_{\text{pseudo}}) \rangle^{\text{peptide}}$ on the same apparatus and with the same procedures (equation S5).^{73,84} The finishing procedure prescribed to prepare $\text{Fab-D}_2\text{O}$ for measurements ensures that $\langle m(\infty_{\text{pseudo}}) \rangle^{\text{peptide}}$ is essentially the same for all laboratories; thus, bias in the back-exchange calculation for each coincident peptide ($\omega_i^c \geq 2$) propagates equally across laboratories. Since such bias does not adversely affect the present determination of HDX-MS precision, the present results are suitable for computing the reproducibility of HDX-MS.

Intact protein mass spectrometry of Fab of NISTmAb reveals the possibility of nascent amide protons that are effectively unavailable for exchange (see Supporting Information); hence, $\langle m(\infty_{\text{pseudo}}) \rangle^{\text{peptide}} < \langle m(\infty) \rangle^{\text{peptide}}$ for a fraction of the peptides. Consequently, the $\%E_{\text{corrected}}^{\text{peptide}}(t_{\text{HDX}})$ values reported herein are not reference values for the Fab fragment of NISTmAb. The distribution of sequestered protons along the protein polymer is likely inhomogeneous.

The main effects study reveals that the peptides reported by the cohort exhibit significant deuterium loss between the first and third chromatographic gradients (reps) conducted for a run. Since the loss of deuterium exchange is observed in $\%E_{\text{corrected}}^{\text{peptide}}$ and $\%E_{\text{uncorrected}}^{\text{peptide}}$ equally, the diminished response may evidence incomplete removal of peptides from the chromatographic apparatus between the replicate measurements. Adverse effects of carryover have been reported previously, and the magnitude of these effects can vary by peptide composition and column chemistry.^{80,81} Diversity of the carryover contribution across laboratories increases the uncertainty of $\%E_{\text{corrected}}^{\text{peptide}}$. Thus, minimization of carryover is essential for precise HDX-MS measurements.

The laboratory cohort reported peptide sequences with a coincidence frequency distribution containing 245 sequences of $\omega_i^c = 1$ and 185 sequences of coincidence frequencies of $2 \leq \omega_i^c \leq 15$ (Figure S5). In view of the diverse operating conditions of the protease columns (Tables S4 and S5), the importance of this result is uncertain.

Still, proteomics studies have reported that series of pepsin digests conducted under the same conditions display a great diversity of sequences and the prevalence of unique sequences ($\omega_i^c = 1$).^{85,86} For example, Ahn et al. reported peptide identifications for a series of 31 digestions conducted at the same pH, salt concentration, temperature, and flow rate.⁸⁶ They found that a few (ubiquitous) peptides appeared in every

digestion and that other peptides appeared only once in the digestion series. Unique peptic peptides outnumbered the reproducible peptides, and the number of unique peptides increased with each consecutive digestion. The number of reproducible peptides plateaued above five to six replicate digestions. In their study, a peptide was defined as “reproducible” when it appeared in 50% of digestions.

The similar populations of $\omega_i^c = 1$ and $\omega_i^c > 1$ sequences and the rapid falloff of coincidence population $M(\omega^c)$ to single-digit coincidence frequency ω^c (Figure S5) suggest that the distribution of coincident sequences may follow a modified binomial function.⁸⁷ In silico digestion by pepsin of the light and heavy chains of Fab of NISTmAb generates a powerset of nearly 8100 peptide sequences containing 4 to 30 amino acids. (This calculation used the constraints that pepsin does not cleave at the P1 position for H, K, R, and P, nor at the P2 for P.⁸⁸) When sample sizes are small compared to the total number of possible sequences, binomial functions predict that the number of unique sequences ($\omega_i^c = 1$) will be greater than the number of sequences of higher coincidence frequency ($\omega_i^c > 1$), as reported in this study. For the sample sizes reported by the laboratory cohort, most binomial models predict that no peptide sequence will manifest a coincidence frequency of $\omega_i^c > 6$.

Cleavage bias of pepsin and instrument fitness may also produce subset populations of ubiquitous sequences, δ_w that exhibit sufficient signal-to-noise ratio (S/N) for HDX-MS measurements by most laboratories. The ubiquitous sequences may account for the small set of peptide sequences with coincidence frequencies ranging $6 \leq \omega_i^c \leq 15$ (Figure S5). Thus, a modified binomial function may exist that can account for the $M(\omega^c)$ versus ω^c distribution found for the laboratory cohort.

The plethora of peptic sequences produced from the Fab fragment may cause chromatographic crowding, confounding identifications. The surfeit of species may also result in ion suppression in the electrospray source of less abundant and difficult to ionize peptides. Dependent upon operating conditions and instrument fitness, peptides exhibiting marginal S/N may sporadically fall just within and just outside acceptance criteria for centroid determinations. For proteomics measurements of the same protein, each laboratory of the cohort may acquire a distinct subset of observed peptide sequences. Sequences within each subset may appear to be selected randomly from the powerset.

Inspection of Figure 2 shows that at least 32 sequences must be measured in order to describe 95% of the Fab of NISTmAb HDX dynamics. For the quality control of a biotherapeutic product based solely on sequence-level comparisons of the deuterium content, the somewhat stochastic behavior of pepsin will add complexity, as not all sequences may be available during a measurement campaign. The quality control laboratory will usually observe the subset of ubiquitous sequences δ_u consistently, but the laboratory will likely need to repeat digestions, until the necessary peptides are measured.

CONCLUSION

The NIST HDX-MS interlaboratory comparison project has analyzed 15 HDX-MS data sets ($\sim 78\,900$ centroids) for the Fab fragment of NISTmAb reference material. This study finds that most laboratories achieve a measurement repeatability precision of $\langle s^{\text{Lab}} \rangle \leq 0.15 \pm 0.01 \text{ Da}$ ($1\sigma_{\bar{x}}$). Plots of repeatability can help assess HDX-MS system fitness and reveal procedural problems. Bottom-up HDX-MS generally has a reproducibility of $\sigma_{\text{reproducibility}}^{15 \text{ Laboratories}} = (9.0 \pm 0.9) \%$. The distribution of peptic peptides

reported by the laboratory cohort exhibit relatively few coincidences. This low coincidence frequency distribution may require quality control methods based on bottom-up HDX-MS to perform repeated measurements to acquire a suitable number of peptides.

■ ASSOCIATED CONTENT

📄 Supporting Information

The Supporting Information is available free of charge on the ACS Publications website at DOI: 10.1021/acs.analchem.9b01100.

Descriptions of materials, metrological methods, computational methods, and supplementary results. Figures of HDX-MS publications and citations versus publication year, histogram of peptide sequence lengths, sequence coverage maps, performance of instrument-software configurations, repeatability plots, $\%E_{\text{corrected}}^{\text{peptide}}(t_{\text{HDX}})$ versus $\log_{10}(t_{\text{HDX}})$ for eight peptides. Tables of instrumentation, software, peptide search methodology, and operating conditions of proteolytic, chromatographic components, and effects of peptide charge on deuterium uptake (PDF)

■ AUTHOR INFORMATION

Corresponding Author

*E-mail: jeffrey.hudgens@nist.gov.

ORCID

Jeffrey W. Hudgens: 0000-0003-2805-1048
Elyssia S. Gallagher: 0000-0002-5411-7285
Ioannis Karageorgos: 0000-0002-2799-766X
Kyle W. Anderson: 0000-0002-2808-3026
James J. Filliben: 0000-0002-2388-3198
Richard Y.-C. Huang: 0000-0002-7172-110X
Guodong Chen: 0000-0002-5531-407X
George M. Bou-Assaf: 0000-0003-4285-5915
Alfonso Espada: 0000-0002-8301-1201
Michael J. Chalmers: 0000-0002-2139-6089
Eduardo Harguindevy: 0000-0002-9291-0591
Hui-Min Zhang: 0000-0002-2099-4730
Benjamin T. Walters: 0000-0001-5400-0696
Jennifer Zhang: 0000-0002-9036-0477
John Venable: 0000-0002-9938-4643
Inhee Park: 0000-0001-9161-438X
Ansgar Brock: 0000-0002-8080-3107
Xiaojun Lu: 0000-0001-5251-4343
Ratnesh Pandey: 0000-0002-0072-6480
Arun Chandramohan: 0000-0002-4175-5886
Ganesh Srinivasan Anand: 0000-0001-8995-3067
Sasidhar N. Nirudodhi: 0000-0002-1827-7177
Justin B. Sperry: 0000-0002-3274-2194
Jason C. Rouse: 0000-0002-2721-7264
James A. Carroll: 0000-0001-6790-0087
Kasper D. Rand: 0000-0002-6337-5489
Ulrike Leurs: 0000-0002-8828-3505
David D. Weis: 0000-0003-3032-1211
Mohammed A. Al-Naqshabandi: 0000-0003-0839-5636
Tyler S. Hageman: 0000-0003-0112-8893
Daniel Deredge: 0000-0002-6897-6523
Patrick L. Wintrobe: 0000-0003-1866-9397
Malvina Papanastasiou: 0000-0003-3378-6612

John D. Lambris: 0000-0002-9370-5776

Sheng Li: 0000-0002-9073-6809

Sarah Urata: 0000-0001-7512-4081

Present Addresses

✉ Baylor University, Department of Chemistry and Biochemistry, One Bear Place #97348, Waco, TX 76798, United States. E-mail: Elyssia_Gallagher@baylor.edu.

► The Rockefeller University, Proteomics Resource Center, 1230 York Avenue New York, NY 10065-6399, United States. E-mail: Caitlin.Steckler@Rockefeller.edu.

✉ Computer Science, San Jose State University, San Jose, CA 95192, United States. E-mail: inhee.park@sjsu.edu.

✉ Adimab LLC, 7 Lucent Drive, Lebanon, NH 03766, United States. E-mail: lxj_cwru@yahoo.com

✉ GSK Vaccines, 14200 Shady Grove Road, Rockville, MD 20850, United States. E-mail: ratnesh.k.pandey@gsk.com

✉ Merck, Sharp, & Dohme Corporation, 50 Tuas West Drive, Singapore 638408. E-mail: arun.chandramohan@merck.com.

✉ Blegdamsvej 3B, Mærsk Tower floor 9, Department of Biomedical Sciences, Faculty of Health and Medical Sciences, University of Copenhagen, Denmark. E-mail: ulrike.leurs@sund.ku.dk.

✉ Broad Institute of MIT & Harvard, 415 Main Street, Cambridge, MA 02142, United States. E-mail: malpap@broadinstitute.org.

✉ E-mail: sarah.urata@gmail.com.

Author Contributions

✉ These authors contributed equally. The manuscript was written through contributions of all authors. All authors have given approval to the final version of the manuscript.

Funding

The NIST project (design, test reagents, data analysis, and manuscript preparation) was funded by the NIST Biomanufacturing Program, and the project design precludes the presence of competing financial interests. C.S. was supported by the National Institute of General Medical Sciences of the National Institutes of Health (NIH), Award No. U54 GM094586. G.S.A. was supported by grants from the Singapore Ministry of Education Academic Research Fund Tier 3 (No. MOE2012-T3-1-008). K.D.R. acknowledges financial support from the Danish Council for Independent Research (Sapere Aude Grant No. DFF-4184-00537A). D.D. and P.W. declare that work at their institution was supported in part by the Univ. of Maryland Baltimore, School of Pharmacy Mass Spectrometry Center (SOP1841-IQB2014). M.P. and J.D.L. declare that work conducted at their institution was supported by National Institutes of Health (Grant Nos. AI068730 and AI030040).

Notes

Disclaimer: Certain commercial materials and equipment are identified to adequately specify experimental procedures. Such identifications neither imply recommendation or endorsement by the National Institute of Standards and Technology nor does it imply that the material or equipment identified is the best available for the purpose.

The authors declare no competing financial interest.

■ ACKNOWLEDGMENTS

J.W.H. at NIST wishes to acknowledge Dr. D. Ripple for his advice on procedures and legal hurdles, Dr. A. L. Rukhin for discussions on probability problems, Ms. T. Solomon for her assistance with experiments, and Ms. N. McDonald for assistance with the composition analysis software and data

archival. J.W.H. also thanks Dr. Y. Hamuro for insightful discussions. I.K., E.S.G., and K.W.A. of NIST and IBBR acknowledge support from the NIST National Research Council (NRC) Postdoctoral Research Associateship Program. R.Y.C.H. and G.C. of Bristol-Myers Squibb acknowledge Dr. A. Tymiak and Dr. B. Car for their support of this project. A.E. and E.H. at Centro de Investigación Lilly, S.A., acknowledge Mr. S. Cano for technical assistance. H.M.Z., B.W., and J.Z. at Genentech, Inc. acknowledge Dr. Y.-H. Kao and Dr. J. Stults for their support for this project. X.L. and R.P. of MedImmune LLC acknowledge Dr. Q. (Paula) Lei and Dr. M. Washabaugh for their support for this study. D.D.W. at Univ. of Kansas acknowledges Agilent Technologies for an equipment loan.

REFERENCES

- (1) Weis, D. D. *Hydrogen Exchange Mass Spectrometry of Proteins: Fundamentals, Methods, and Applications*, 1st ed.; John Wiley & Sons, Ltd.: Chichester, UK, 2016.
- (2) *Web of Science Database Search on HDX-MS of proteins and peptides (no reviews or commentary)*; Clarivate Analytics: Philadelphia, PA, 2019; accessed Feb 18, 2019.
- (3) Google Patents; Alphabet Corp., 2017; accessed Sept 25, 2017.
- (4) Rogstad, S.; Faustino, A.; Ruth, A.; Keire, D.; Boyne, M.; Park, J. J. *Am. Soc. Mass Spectrom.* **2017**, *28* (5), 786–794.
- (5) Gutierrez-Lugo, M. T. Regulatory Consideration for the Characterization of HOS in Biotechnology Products. In *HOS 2016, Fifth International Symposium on Higher Order Structure of Protein Therapeutics*, Long Beach, CA, April 11–13, 2016; Olson, R., Ed.; CASSS: Long Beach, CA, 2016.
- (6) Iacob, R. E.; Engen, J. R. *J. Am. Soc. Mass Spectrom.* **2012**, *23* (6), 1003–1010.
- (7) Houde, D.; Berkowitz, S. A.; Engen, J. R. *J. Pharm. Sci.* **2011**, *100* (6), 2071–2086.
- (8) Berkowitz, S. A.; Engen, J. R.; Mazzeo, J. R.; Jones, G. B. *Nat. Rev. Drug Discovery* **2012**, *11* (7), 527–540.
- (9) Wei, H.; Ahn, J.; Yu, Y. Q.; Tymiak, A.; Engen, J. R.; Chen, G. J. *Am. Soc. Mass Spectrom.* **2012**, *23* (3), 498–504.
- (10) Visser, J.; Feuerstein, I.; Stangler, T.; Schmiederer, T.; Fritsch, C.; Schiestl, M. *BioDrugs* **2013**, *27* (5), 495–507.
- (11) Iacob, R. E.; Chen, G.; Ahn, J.; Houel, S.; Wei, H.; Mo, J.; Tao, L.; Cohen, D.; Xie, D.; Lin, Z.; Morin, P. E.; Doyle, M. L.; Tymiak, A. A.; Engen, J. R. *J. Am. Soc. Mass Spectrom.* **2014**, *25* (12), 2093–2102.
- (12) Beck, A.; Debaene, F.; Diemer, H.; Wagner-Rousset, E.; Colas, O.; Van Dorsselaer, A.; Cianferani, S. *J. Mass Spectrom.* **2015**, *50* (2), 285–297.
- (13) Pan, J.; Borchers, C. H. *Proteomics* **2014**, *14* (10), 1249–1258.
- (14) Leurs, U.; Mistarz, U. H.; Rand, K. D. *Eur. J. Pharm. Biopharm.* **2015**, *93*, 95–109.
- (15) Campobasso, N.; Huddler, D. *Bioorg. Med. Chem. Lett.* **2015**, *25* (18), 3771–3776.
- (16) Majumdar, R.; Esfandiary, R.; Bishop, S. M.; Samra, H. S.; Middaugh, C. R.; Volkin, D. B.; Weis, D. D. *mAbs* **2015**, *7* (1), 84–95.
- (17) Iacob, R. E.; Krystek, S. R.; Huang, R. Y. C.; Wei, H.; Tao, L.; Lin, Z.; Morin, P. E.; Doyle, M. L.; Tymiak, A. A.; Engen, J. R.; Chen, G. *Expert Rev. Proteomics* **2015**, *12* (2), 159–169.
- (18) Deng, B.; Lento, C.; Wilson, D. J. *Anal. Chim. Acta* **2016**, *940*, 8–20.
- (19) Pan, J.; Zhang, S.; Chou, A.; Borchers, C. H. *Chemical Science* **2016**, *7* (2), 1480–1486.
- (20) Nazari, Z. E.; van de Weert, M.; Bou-Assaf, G.; Houde, D.; Weiskopf, A.; Rand, K. D. *J. Pharm. Sci.* **2016**, *105* (11), 3269–3277.
- (21) Iacob, R. E.; Engen, J. R.; Krull, I. S.; Rathore, A. *LC GC North America* **2017**, *35* (6), 382–390.
- (22) Masson, G. R.; Jenkins, M. L.; Burke, J. E. *Expert Opin. Drug Discovery* **2017**, *12* (10), 981–994.
- (23) Huang, R. Y. C.; Iacob, R. E.; Krystek, S. R.; Jin, M.; Wei, H.; Tao, L.; Das, T. K.; Tymiak, A. A.; Engen, J. R.; Chen, G. D. *J. Am. Soc. Mass Spectrom.* **2017**, *28* (5), 795–802.
- (24) Huang, R. Y.-C.; Chen, G. *Anal. Bioanal. Chem.* **2014**, *406* (26), 6541–6558.
- (25) Nirudodhi, S. N.; Sperry, J. B.; Rouse, J. C.; Carroll, J. A. *J. Pharm. Sci.* **2017**, *106* (2), 530–536.
- (26) Huang, R. Y. C.; Krystek, S. R.; Felix, N.; Graziano, R. F.; Srinivasan, M.; Pashine, A.; Chen, G. *mAbs* **2018**, *10* (1), 95–103.
- (27) Englander, S. W. *Annu. Rev. Biophys. Biomol. Struct.* **2000**, *29*, 213–238.
- (28) Hoofnagle, A. N.; Resing, K. A.; Ahn, N. G. *Annu. Rev. Biophys. Biomol. Struct.* **2003**, *32*, 1–25.
- (29) Lu, X. J.; Wintrobe, P. L.; Surewicz, W. K. *Proc. Natl. Acad. Sci. U. S. A.* **2007**, *104* (5), 1510–1515.
- (30) Konermann, L.; Pan, J. X.; Liu, Y. H. *Chem. Soc. Rev.* **2011**, *40* (3), 1224–1234.
- (31) Engen, J. R.; Wales, T. E.; Chen, S. G.; Marzluff, E. M.; Hassell, K. M.; Weis, D. D.; Smithgall, T. E. *Int. Rev. Phys. Chem.* **2013**, *32* (1), 96–127.
- (32) Shukla, A. K.; Westfield, G. H.; Xiao, K. H.; Reis, R. I.; Huang, L. Y.; Tripathi-Shukla, P.; Qian, J.; Li, S.; Blanc, A.; Oleskie, A. N.; Dosey, A. M.; Su, M.; Liang, C. R.; Gu, L. L.; Shan, J. M.; Chen, X.; Hanna, R.; Choi, M. J.; Yao, X. J.; Klink, B. U.; Kahsai, A. W.; Sidhu, S. S.; Koide, S.; Penczek, P. A.; Kossiakoff, A. A.; Woods, V. L.; Kobilka, B. K.; Skiniotis, G.; Lefkowitz, R. J. *Nature* **2014**, *512* (7513), 218.
- (33) Englander, S. W.; Mayne, L.; Kan, Z. Y.; Hu, W. B. *Annu. Rev. Biophys.* **2016**, *45*, 135–152, DOI: 10.1146/annurev-biophys-062215-011121.
- (34) Adhikary, S.; Deredge, D. J.; Nagarajan, A.; Forrest, L. R.; Wintrobe, P. L.; Singh, S. K. *Proc. Natl. Acad. Sci. U. S. A.* **2017**, *114* (10), E1786–E1795.
- (35) Papanastasiou, M.; Koutsogiannaki, S.; Sarigiannis, Y.; Geisbrecht, B. V.; Ricklin, D.; Lambiris, J. D. *J. Immunol.* **2017**, *198* (8), 3326–3335.
- (36) Pirrone, G. F.; Iacob, R. E.; Engen, J. R. *Anal. Chem.* **2015**, *87* (1), 99–118.
- (37) Bereszcak, J. Z.; Rose, R. J.; van Duijn, E.; Watts, N. R.; Wingfield, P. T.; Steven, A. C.; Heck, A. J. R. *J. Am. Chem. Soc.* **2013**, *135* (17), 6504–6512.
- (38) Bereszcak, J. Z.; Watts, N. R.; Wingfield, P. T.; Steven, A. C.; Heck, A. J. R. *Protein Sci.* **2014**, *23* (7), 884–896.
- (39) Snijder, J.; Benevento, M.; Moyer, C. L.; Reddy, V.; Nemerow, G. R.; Heck, A. J. R. *J. Mol. Biol.* **2014**, *426* (9), 1971–1979.
- (40) Wijesinghe, K. J.; Urata, S.; Bhattacharai, N.; Kooijman, E. E.; Gerstman, B. S.; Chapagain, P. P.; Li, S.; Stahelin, R. V. *J. Biol. Chem.* **2017**, *292* (15), 6108–6122.
- (41) Johnson, B.; Li, J.; Adhikari, J.; Edwards, M. R.; Zhang, H.; Schwarz, T.; Leung, D. W.; Basler, C. F.; Gross, M. L.; Amarasinghe, G. K. *J. Mol. Biol.* **2016**, *428* (17), 3483–3494.
- (42) Lim, X. X.; Chandramohan, A.; Lim, X. Y. E.; Bag, N.; Sharma, K. K.; Wirawan, M.; Wohland, T.; Lok, S. M.; Anand, G. S. *Nat. Commun.* **2017**, *8*, 14339.
- (43) Noble, A. J.; Zhang, Q.; O'Donnell, J.; Hariri, H.; Bhattacharya, N.; Marshall, A. G.; Stagg, S. M. *Nat. Struct. Mol. Biol.* **2013**, *20* (2), 167–173, DOI: 10.1038/nsmb.2467.
- (44) Marriott, J.; O'Connor, G.; Parkes, H. Study of Measurement Service and Comparison Needs for an International Measurement Infrastructure for the Biosciences and Biotechnology: Input for the BIPM Work Programme <http://www.bipm.org/utis/common/pdf/rapportBIPM/2011/02.pdf> (accessed June 9, 2018).
- (45) Wei, H.; Mo, J. J.; Tao, L.; Russell, R. J.; Tymiak, A. A.; Chen, G. D.; Iacob, R. E.; Engen, J. R. *Drug Discovery Today* **2014**, *19* (1), 95–102.
- (46) JGCM 200:2012 International vocabulary of metrology—Basic and general concepts and associated terms (VIM) Joint Committee for Guides in Metrology 2012. (2008 edn with minor corrections) ed.; Bureau International des Poids et Mesures: Cedex, France, 2012. <http://www.bipm.org/en/publications/guides/vim.html>.

- (47) Menditto, A.; Patriarca, M.; Magnusson, B. *Accredit. Qual. Assur.* **2007**, *12* (1), 45–47.
- (48) Petruk, A. A.; Defelipe, L. A.; Rodríguez Limardo, R. G.; Bucci, H.; Marti, M. A.; Turjanski, A. G. *J. Chem. Theory Comput.* **2013**, *9* (1), 658–669.
- (49) McAllister, R. G.; Konermann, L. *Biochemistry* **2015**, *54* (16), 2683–2692.
- (50) Borysik, A. J. *Angew. Chem., Int. Ed.* **2017**, *56* (32), 9396–9399.
- (51) Mazur, S. J.; Gallagher, E. S.; Debnath, S.; Durell, S. R.; Anderson, K. W.; Miller Jenkins, L. M.; Appella, E.; Hudgens, J. W. *Biochemistry* **2017**, *56* (21), 2676–2689.
- (52) Boon, P. L. S.; Saw, W. G.; Lim, X. X.; Raghuvamsi, P. V.; Huber, R. G.; Marzinek, J. K.; Holdbrook, D. A.; Anand, G. S.; Grüber, G.; Bond, P. J. *ACS Chem. Biol.* **2018**, *13* (6), 1621–1630.
- (53) Mohammadiarani, H.; Shaw, V. S.; Neubig, R. R.; Vashisth, H. J. *Phys. Chem. B* **2018**, *122* (40), 9314–9323.
- (54) Markwick, P. R. L.; Peacock, R. B.; Komives, E. A. *Biophys. J.* **2019**, *116* (1), 49–56.
- (55) Chalmers, M. J.; Busby, S. A.; Pascal, B. D.; He, Y.; Hendrickson, C. L.; Marshall, A. G.; Griffin, P. R. *Anal. Chem.* **2006**, *78* (4), 1005–1014.
- (56) Burkitt, W.; O'Connor, G. *Rapid Commun. Mass Spectrom.* **2008**, *22* (23), 3893–3901.
- (57) Chalmers, M. J.; Pascal, B. D.; Willis, S.; Zhang, J.; Iturria, S. J.; Dodge, J. A.; Griffin, P. R. *Int. J. Mass Spectrom.* **2011**, *302* (1–3), 59–68.
- (58) Hudgens, J. W.; Huang, R. Y.-C.; D'Ambro, E. Method Validation and Standards in Hydrogen Exchange Mass Spectrometry. In *Hydrogen Exchange Mass Spectrometry of Proteins: Fundamentals, Methods, and Applications*, 1st ed.; Weis, D. D., Ed.; John Wiley & Sons, Ltd.: Chichester, UK, 2016; pp 55–72.
- (59) Cummins, D. J.; Espada, A.; Novick, S. J.; Molina-Martin, M.; Stites, R. E.; Espinosa, J. F.; Broughton, H.; Goswami, D.; Pascal, B. D.; Dodge, J. A.; Chalmers, M. J.; Griffin, P. R. *Anal. Chem.* **2016**, *88* (12), 6607–6614.
- (60) Gallagher, E. S.; Hudgens, J. W. *Methods Enzymol.* **2016**, *566*, 357–404.
- (61) Engen, J. R. *Analyst* **2003**, *128* (6), 623–628.
- (62) Engen, J. R.; Wales, T. E. *Annu. Rev. Anal. Chem.* **2015**, *8*, 127–148, DOI: 10.1146/annurev-anchem-062011-143113.
- (63) Hamuro, Y.; Coales, S. J. *J. Am. Soc. Mass Spectrom.* **2018**, *29* (3), 623–629.
- (64) Marino, J. P.; Brinson, R. G.; Hudgens, J. W.; Ladner, J. E.; Gallagher, D. T.; Gallagher, E. S.; Arbogast, L. W.; Huang, R. Y. C. Emerging Technologies To Assess the Higher Order Structure of Monoclonal Antibodies. In *State-of-the-Art and Emerging Technologies for Therapeutic Monoclonal Antibody Characterization, Volume 3: Defining the Next Generation of Analytical and Biophysical Techniques*; Schiel, J. E., Davis, D. L., Borisov, O. V., Eds.; ACS Symposium Series 1202; American Chemical Society: Washington, DC, 2015; pp 17–43.
- (65) Karageorgos, I.; Gallagher, E. S.; Galvin, C.; Gallagher, D. T.; Hudgens, J. W. *Biologicals* **2017**, *50*, 27–34.
- (66) Gallagher, D. T.; Karageorgos, I.; Hudgens, J. W.; Galvin, C. V. *Data in Brief* **2018**, *16*, 29–36.
- (67) Zhang, H. M.; McLoughlin, S. M.; Frausto, S. D.; Tang, H. L.; Emmett, M. R.; Marshall, A. G. *Anal. Chem.* **2010**, *82* (4), 1450–1454.
- (68) Bai, Y. W.; Milne, J. S.; Mayne, L.; Englander, S. W. *Proteins: Struct., Funct., Genet.* **1993**, *17* (1), 75–86.
- (69) Cravello, L.; Lascoux, D.; Forest, E. *Rapid Commun. Mass Spectrom.* **2003**, *17* (21), 2387–2393.
- (70) Hamuro, Y.; Zhang, T. J. *Am. Soc. Mass Spectrom.* **2019**, *30*, 227–234.
- (71) Hvidt, A.; Nielsen, S. O., Hydrogen Exchange in Proteins. In *Advances in Protein Chemistry*; Anfinsen, C. B., Anson, M. L., Edsall, J. T., Richards, F. M., Eds.; Academic Press, 1966; Vol. 21, pp 287–386.
- (72) Englander, S. W.; Kallenbach, N. R. Q. *Rev. Biophys.* **1983**, *16* (4), 521–655.
- (73) Mayne, L., Hydrogen Exchange Mass Spectrometry. In *Methods in Enzymology*; Kelman, Z., Ed.; Academic Press, 2016; Vol. 566, pp 335–356.
- (74) Hudgens, J. W.; Gallagher, E. S.; Karageorgos, I.; Anderson, K. W.; Huang, R. Y.-C.; Chen, G.; Bou-Assaf, G. M.; Espada, A.; Chalmers, M. J.; Harguindeguy, E.; Zhang, H.-M.; Walters, B. T.; Zhang, J.; Venable, J.; Steckler, C.; Park, I.; Brock, A.; Lu, X.; Pandey, R.; Chandramohan, A.; Srinivasan Anand, G.; Nirudodhi, S. N.; Sperry, J. B.; Rouse, J. C.; Carroll, J. A.; Rand, K. D.; Leurs, U.; Weis, D. D.; Al-Naqshabandi, M. A.; Hageman, T. S.; Deredge, D.; Wintrode, P. L.; Papanastasiou, M.; Lambris, J. D.; Li, S.; Urata, S. *J. Res. NIST* **2019**, *124*, 124009.
- (75) Kostyukevich, Y.; et al. *J. Mass Spectrom.* **2014**, *49* (10), 989–994.
- (76) Kim, H. J.; Liyanage, O. T.; Mullen, M. R.; Gallagher, E. S. *J. Am. Soc. Mass Spectrom.* **2018**, *29*, 2030.
- (77) Filliben, J. J.; Tobias, P.; Trutna, L., Design of Experiments (DOE) Mean Plot. In *NIST/SEMATECH e-Handbook of Statistical Methods*; National Institute of Standards and Technology, 2003. Online at <https://www.itl.nist.gov/div898/handbook/>.
- (78) Heckert, N. A.; Filliben, J. J. *Dataplot*; NIST; online at <http://www.itl.nist.gov/div898/software/dataplot/>. Accessed Oct 4, 2017.
- (79) Filliben, J. J. *DATA PLOT—Introduction and Overview*, NIST Special Publication 667 pdf version. National Bureau of Standards: Gaithersburg, MD, 1984. <http://www.itl.nist.gov/div898/software/dataplot/sp667.pdf>.
- (80) Fang, J.; Rand, K. D.; Beuning, P. J.; Engen, J. R. *Int. J. Mass Spectrom.* **2011**, *302* (1–3), 19–25.
- (81) Majumdar, R.; Manikwar, P.; Hickey, J. M.; Arora, J.; Middaugh, C. R.; Volkin, D. B.; Weis, D. D. *J. Am. Soc. Mass Spectrom.* **2012**, *23* (12), 2140–2148.
- (82) Jensen, P. F.; Rand, K. D., Hydrogen Exchange: A Sensitive Analytical Window into Protein Conformation and Dynamics. In *Hydrogen Exchange Mass Spectrometry of Proteins: Fundamentals, Methods, and Applications*, 1st ed.; Weis, D. D., Ed.; John Wiley & Sons, Ltd.: Chichester, UK, 2016; pp 1–17.
- (83) Zhang, Z.; Fang, J. Extracting Information from Hydrogen Exchange Mass Spectrometry Data. In *Hydrogen Exchange Mass Spectrometry of Proteins: Fundamentals, Methods, and Applications*, 1st ed.; Weis, D. D., Ed.; John Wiley & Sons, Ltd.: Chichester, UK, 2016; pp 107–125.
- (84) Zhang, Z.; Smith, D. L. *Protein Sci.* **1993**, *2*, 522–531.
- (85) López-Ferrer, D.; Petritis, K.; Robinson, E. W.; Hixson, K. K.; Tian, Z.; Lee, J. H.; Lee, S.-W.; Tolić, N.; Weitz, K. K.; Belov, M. E.; Smith, R. D.; Paša-Tolić, L. *Mol. Cell. Proteomics* **2011**, *10* (2), M110001479.
- (86) Ahn, J.; Cao, M.-J.; Yu, Y. Q.; Engen, J. R. *Biochim. Biophys. Acta, Proteins Proteomics* **2013**, *1834* (6), 1222–1229.
- (87) NIST/SEMATECH e-Handbook of Statistical Methods. <https://www.itl.nist.gov/div898/handbook/eda/section3/eda366i.htm>. Accessed June 4, 2018.
- (88) Hamuro, Y.; Coales, S. J.; Molnar, K. S.; Tuske, S. J.; Morrow, J. A. *Rapid Commun. Mass Spectrom.* **2008**, *22* (7), 1041–1046.

Supporting Information for:

Interlaboratory Comparison of Hydrogen-Deuterium Exchange Mass Spectrometry Measurements of the Fab fragment of NISTmAb.

Jeffrey W. Hudgens^{*,†,‡}, Elyssia S. Gallagher^{†,‡}, Ioannis Karageorgos^{†,‡}, Kyle W. Anderson^{†,‡}, James J. Filliben[†], Richard Y.-C. Huang^{*}, Guodong Chen^{*}, George M. Bou-Assaf[‡], Alfonso Espada[#], Michael J. Chalmers[×], Eduardo Harguindeguy[#], Hui-Min Zhang[§], Benjamin T. Walters[§], Jennifer Zhang[§], John Venable^{*}, Caitlin Steckler^{*,⊗}, Inhee Park^{*}, Ansgar Brock^{*}, Xiaojun Lu^{∇,∇}, Ratnesh Pandey^{∇,∇}, Arun Chandramohan[€], Ganesh Srinivasan Anand[€], Sasidhar N. Nirudodhi^ϕ, Justin B. Sperry^Δ, Jason C. Rouse[†], James A. Carroll^Δ, Kasper D. Rand[⊙], Ulrike Leurs[⊙], David D. Weis^γ, Mohammed A. Al-Naqshabandi^{γ,Σ}, Tyler S. Hageman^γ, Daniel Deredge^β, Patrick L. Wintrode^β, Malvina Papanastasiou^Π, John D. Lambris^Π, Sheng Li[&], and Sarah Urata[&]

[†] National Institute of Standards and Technology, Bioprocess Measurement Group, Biomolecular Measurements Division, Rockville, MD, 20850, United States

[‡] Institute for Bioscience and Biotechnology Research, 9600 Gudelsky Drive, Rockville Maryland, 20850, United States

[†] National Institute of Standards and Technology, Statistical Engineering Division, Gaithersburg, Maryland, 20899, United States

^{*} Bristol-Myers Squibb Company, Pharmaceutical Candidate Optimization, Research and Development, Princeton, New Jersey 08540, United States

[‡] Biogen Inc., Analytical Development, 225 Binney Street, Cambridge, Massachusetts 02142, United States

[#] Centro de Investigación Lilly S.A., 28108-Alcobendas, Spain

[×] Lilly Research Laboratories, Eli Lilly and Company, Indianapolis, Indiana 46285, United States

[§] Genentech, Inc. Protein Analytical Chemistry, 1 DNA Way, South San Francisco, California 94080, United States

^{*} Genomics Institute of the Novartis Research Foundation, 10675 John Jay Hopkins Drive, San Diego, California 92121, United States

[⊗] Joint Center for Structural Genomics, La Jolla, California 92037, United States

[∇] MedImmune LLC, One MedImmune Way, Gaithersburg, Maryland 20878, United States

[€] National University of Singapore, Department of Biological Sciences, 14, Science Drive 4, Singapore 117543

^ϕ Pfizer Inc., Vaccine R&D, 401 N Middletown Rd, Pearl River, New York 10965, United States

^Δ Pfizer Inc., Analytical R&D, 700 Chesterfield Parkway West, Chesterfield, Missouri 63017, United States

[†] Pfizer Inc., Analytical R&D, 1 Burtt Road, Andover, Massachusetts 01810, United States

[⊙] University of Copenhagen, Department of Pharmacy, Universitetsparken 2, DK-2100 Copenhagen, Denmark

^γ University of Kansas, Department of Chemistry, 1567 Irving Hill Road, Lawrence, Kansas 66045, United States

^Σ Soran University, Department of General Science, Kawa Street, Soran, Kurdistan Region, Iraq

^β University of Maryland, Baltimore, School of Pharmacy, Department of Pharmaceutical Sciences, 20 North Pine Street, Baltimore, Maryland 21201, United States

^Π University of Pennsylvania, Department of Pathology & Laboratory Medicine, Perelman School of Medicine, 402 Stellar-Chance Labs, 422 Curie Boulevard, Philadelphia, Pennsylvania 19104-6100, United States

[&] University of California, San Diego, Department of Medicine, 9500 Gilman Drive, La Jolla, California 92093, United States

Table of Contents

SUPPORTING INFORMATION	S-3
MATERIALS	S-3
Reagents and Materials.	S-3
HDX-MS Kit.	S-3
Onsite Preparation of Fab-H ₂ O Samples.	S-4
Onsite Finishing of Fab-D ₂ O Control Samples	S-4
METROLOGICAL METHODS	S-4
pH measurements.	S-4
Intact Mass Analysis of Fab of NISTmAb.	S-5
Instrumentation	S-5
COMPUTATIONAL METHODS	S-5
Computation of the deuterium uptake by a peptide	S-5
Software and calculation of uncertainty.	S-6
SUPPORTING RESULTS	S-7
Intact Mass Spectrometry of Finished Fab-D ₂ O Samples	S-7
Calculation of repeatability, s^{Lab}	S-7
Using Repeatability plots to assess instrument fitness.	S-7
Effects of peptide charge on deuterium uptake	S-8
FIGURES	S-10
Figure S1. Plot of the number of original research publications (i.e., reviews and commentaries are uncounted) per year that employed HDX-MS to investigate protein behavior.	S-10
Figure S2. The HDX-MS standard reagent kit.	S-11
Figure S3. Histogram showing the observation frequency vs peptide amino acid length (AA).	S-12
Figure S4. Peptide sequences for the heavy chain (HC) and light chain (LC) reported	S-13
Figure S5. Sequence coincidence population $M(\omega^c)$ vs. Coincidence Frequency (ω^c) for sequences reported by the 15 laboratory cohort.	S-17
Figure S6. Population of reported peptide sequences as a function of instrument-software configuration.	S-17
Figure S7. The repeatability plots (s^{peptide} vs t_{HDX}).	S-18
Figure S8. Plots of % $E_{\text{corrected peptide}}(t_{\text{HDX}})$ vs $\log_{10}(t_{\text{HDX}})$ for peptides measured at $T_{\text{HDX}} = (25 \pm 1)^\circ\text{C}$	S-20
TABLES	S-21
Table S1. Positions, vial labeling, and chemical information for each vial in the HDX-MS kit.	S-21

Table S2. Instrument-software configurations used by laboratories to analyze and identify peptide ions.....	S-22
Table S3. Software search engines and parameters used for identifying the peptide ions, as reported by each laboratory.	S-23
Table S4. Proteolytic and chromatography columns and additional conditions reported by each laboratory ...	S-24
Table S5. Physio-chem and fluidic conditions reported by each laboratory for HDX-MS measurements.....	S-28
Table S6. Table of relative $A_z^{\text{total}} = \int \%D_z^{\text{peptide}}(t_{\text{HDX}})d\log_{10}(t_{\text{HDX}})$ integrated over $t_{\text{HDX}} = (3,600 \text{ s}, 14,400 \text{ s}, \infty_{\text{pseudo}})$...	S-29
REFERENCES	S-35

SUPPORTING INFORMATION

MATERIALS

Reagents and Materials. All reagents used to prepare samples and supplied with the HDX-MS kits originated from the same chemical lots. D₂O (99.96 mole % D) was acquired from Cambridge Isotopes (Andover, MA). Sodium phosphate dihydrate, sodium phosphate monohydrate, and sodium chloride were purchased from Sigma-Aldrich (St. Louis, MO). Tris(2-carboxyethyl)phosphine hydrochloride (TCEP) and 98 % guanidine hydrochloride (GdmCl) were acquired from Thermo Scientific (Thermo Fisher Scientific, Pittsburgh, PA).

The test protein for the HDX-MS interlaboratory comparison was the Fab fragment that was enzymatically cleaved from Candidate RM 8670 (Lot #5F1b), which has the same structure as the Fab of the NIST IgG1k reference material, NISTmAb.¹⁻³ Material used for this study contained a small fraction of free Fc fragment. Triple-angle light scattering data indicated that the Fab fragment of NISTmAb sample was in a monomeric state.²⁻³

Samples of Fab fragment were used to prepare Fab-H₂O and Fab-D₂O buffered stock solutions. Fab-D₂O solution was prepared by resuspending lyophilized Fab fragment of NISTmAb in buffered, 99.96 % D₂O. Separate HDX-MS experiments revealed negligible differences between freshly prepared Fab-H₂O and Fab solutions prepared by resuspending lyophilized Fab fragment of NISTmAb in buffered H₂O (data not shown). The Fab-H₂O and Fab-D₂O solutions were dispensed through a 0.2 µm filter into 1 mL glass vials.

HDX-MS Kit. The NIST HDX-MS standard reagent kit comprising a padded box and 26 vials (Figure S2 and Table S1) contained all solutions and materials necessary for generating reference peptide data; for conducting three runs of HDX-MS kinetics studies involving immersion of Fab in buffered D₂O for selected durations, t_{HDX} (Figure 1A); and for quenching the H/D exchange process, denaturing the protein, and reducing disulfide bonds during the analysis process (Figure 1B).

Each kit contained a glass vial holding ≈200 µL Fab–H₂O and a glass vial containing ≈200 µL Fab–D₂O, respectively. Each kit contained one 4 mL glass vial and one 2.5 mL plastic vial of H₂O dilution buffer solution, comprising 20 mmol/L sodium phosphate buffer and 150 mmol/L sodium chloride in deionized H₂O (pH 7.50 ± 0.02). Each kit contained three 4 mL glass vials and one 2.5 mL plastic vial of D₂O

exchange buffer solution, comprising 20 mmol/L sodium phosphate buffer and 150 mmol/L sodium chloride in 99.96 % D₂O (pD_{corrected} 7.48 ± 0.02) ⁴.

Each kit contained four 4 mL glass vials of quench buffer solution, comprising 8 mol/L guanidine-HCl and 0.4 mol/L sodium phosphate in H₂O (pH 3.1 ± 0.02). To assure the preparation of solutions with uniform disulfide bond reducing potential, the kits contained four samples of dry ≈0.70 g tris(2-carboxyethyl) phosphine hydrochloride (TCEP). Each TCEP sample (Pierce™ TCEP; Thermo Scientific, Pittsburgh, PA) was double-sealed within a 1.5 mL Eppendorf tube inside a 5 mL glass vial.

Onsite Preparation of Fab-H₂O Samples. The kit was shipped to participants via an overnight delivery service in an insulated box. The package also contained chemical hazard information, a pamphlet describing the Fab properties and an inventory of the kit contents (Table S1 in the Supporting Information). Dry gel packets maintained the package contents at +4 °C and had sufficient capacity to accommodate transits of at least 48 h. Upon receipt of a package each participant ascertained that the internal temperature was near +4 °C. (Replacement kits were issued to participants upon request.) Using H₂O dilution buffer solution or D₂O exchange buffer solution, as appropriate, laboratories promptly diluted the Fab stock solutions to the concentration suitable for use in HDX-MS studies. Vials were stored at –80 °C until needed.

Prior to this study extensive multi-angle light scattering measurements (MALS) and size-exclusion chromatography (SEC) measurements ascertained that the Fab fragment is resistant to aggregation under stresses typical of refrigerated storage or international shipping on ice. ² Similar measurements found that Fab solutions remain unchanged when stored at -20 °C for eight months and that buffered, pH 7.4 solutions prepared from lyophilized Fab are also the same. Separate HDX-MS experiments revealed negligible differences between freshly prepared Fab-H₂O of NISTmAb and lyophilized Fab fragment of NISTmAb-H₂O resuspended in H₂O.

For a recent study Brinson et al. shipped solutions of Fab fragment of NIST-mAb in NMR sample tubes at +4 °C to 26 laboratories in 9 countries. ⁵ Structural fingerprints as viewed by 2D heteronuclear single quantum coherence (HSQC) proton, nitrogen, and carbon NMR spectroscopy at 500 MHz to 900 MHz showed that the Fab fragment structures were essentially identical, indicating that the shipping process did not alter protein structure.

Onsite Finishing of Fab-D₂O Control Samples. Onsite preparation included additional finishing of the Fab-D₂O control sample to assure that the deuterium content corresponded to $t_{\text{HDX}} \approx \infty_{\text{pseudo}}$ material. At each participating laboratory the Fab-D₂O sample was diluted with 99.96 % D₂O buffered solution to the concentration suitable for the incumbent HDX-MS apparatus. The sample was then incubated at 37 °C for 96 h prior to its centroid measurement. Although this procedure does not assure that the amide sites, (NH)_k, contain 99.96 % D, it does assure that the (NH)_k contains maximum deuterium, as dictated by structural properties.

METROLOGICAL METHODS

pH measurements. During preparation of solutions provided in the HDX-MS kit, pH measurements were conducted with a Thermo-Fisher Model Orion 3-Star Benchtop pH meter (Thermo Scientific, Pittsburgh, PA) coupled to a Catalog# 13-620-223A double junction refillable glass pH Electrode (Fisher Scientific, Pittsburgh, PA). The meter was calibrated using a point-by-point method with four point calibration solutions, pH 1.68, 4.01, 7.00, 10.01 (Oakton Instruments, Vernon Hills, IL).

Intact Mass Analysis of Fab of NISTmAb. Intact masses measurements were obtained for the native Fab fragment of NISTmAb, Fab-H₂O, and for the Fab fragment prepared with maximally-deuterated, exchangeable sites, Fab-D₂O. This Fab-D₂O control sample was finished at each cohort laboratory by incubating Fab-D₂O from the HDX-MS kit at 37 °C for 96 hours in 99.96 % D₂O. Both Fab control samples were infused directly into a Thermo LTQ Orbitrap Elite (Thermo Fisher, San Jose, CA) and an Agilent 6545 Q-TOF (Agilent Technologies, Santa Clara, CA). For these instruments, MagTran 1.03 software (Amgen Inc., Thousand Oaks, CA) ⁶ and BioConfirm 8.0 (Agilent Technologies, Santa Clara, CA), respectively, deconvoluted the resulting spectra. The 1 221.990 637 *m/z* ion of the HP-1221 calibration standard (Agilent Technologies) served as the reference mass for Q-TOF measurements.

Instrumentation. As listed in Table S2 in the participating laboratories employed a variety of hardware and software to manipulate samples, chromatographically separate and mass analyze peptides, and to identify peptide sequences. Table S3 lists the proteolytic, chromatography columns, and chromatography gradient profile used by each laboratory.

COMPUTATIONAL METHODS

Computation of the deuterium uptake by a peptide. The centroid mass observed at time t_{HDX} is determined from peptide isotopic envelope, as observed in the *m/z* spectrum using formula 1:

$$\langle m(t_{\text{HDX}}) \rangle^{\text{peptide}} = z \cdot \left[\frac{\sum_{i=1}^n (m/z_i) \cdot I_i}{\sum_{i=1}^n I_i} - m_{\text{H}^+} \right] \quad (\text{S1})$$

where z is the ion charge, n is the number of isotopic *m/z* features in the mass spectrum of the ion, $(m/z)_i$ is the measured mass to charge ratio, I_i is the intensity of the *i*th ion feature, and m_{H^+} is the proton mass. ⁷ To compute centroids, each reporting laboratory used their chosen software tool. As listed in Table S2 in the Supporting Information, the software included DXMS Explorer and HDExaminer (Sierra Analytics, Modesto, CA), EXMS, ⁸ HDX Workbench, ⁹ and DynamX (Waters Corp., Milford, MA).

At NIST the centroid masses, $\langle m(t_{\text{HDX}}) \rangle$, reported by each laboratory, allowed computation of the deuterium content of the peptide at t_{HDX} from the difference:

$$D^{\text{peptide}}(t_{\text{HDX}}) = \langle m(t_{\text{HDX}}) \rangle^{\text{peptide}} - \langle m(0) \rangle^{\text{peptide}} \quad (\text{S2})$$

where $\langle m(0) \rangle$ is the centroid mass at $t_{\text{HDX}} = 0$ s.

Direct comparisons of peptide data from the laboratories are facilitated by calculating the average percentage of the measured amide sites at t_{HDX} that have exchanged hydrogen for deuterium. At t_{HDX} the average percentage of exchange, uncorrected for back-exchange, is:

$$\%E_{\text{uncorrected}}^{\text{peptide}}(t_{\text{HDX}}) = \frac{D^{\text{peptide}}(t_{\text{HDX}}) \cdot 100 \% }{D_{\text{max}}^{\text{peptide}}} \quad (\text{S3})$$

where $D_{\text{max}}^{\text{peptide}}$ is the maximum molecular weight change due to amide deuteration of a peptide:

$$D_{\max}^{\text{peptide}} = F^{\text{D}_2\text{O}} \cdot (n - p - 2) \cdot (m_{\text{D}^+} - m_{\text{H}^+}) \quad (\text{S4})$$

Here, n is the number of amino acids, p is the number of prolines in the peptide excluding the first one or two N-terminal residues, m_{D^+} is the deuteron mass. Since the present analyses involve extended chromatography in H_2O near 0 °C, the N-terminus and its adjacent amino acid undergo complete back-exchange, and site deuteration of $D_{\max}^{\text{peptide}}$ is reduced by two.¹⁰⁻¹¹

The calculation of $\%E_{\text{corrected}}^{\text{peptide}}(t_{\text{HDX}})$ includes an adjustment for H for D back-exchange during the quench and analysis procedures (Figure 1B to 1E). The present work employs the back-exchange correction specified by Zhang and Smith with the correction for a non-unitary deuterium fraction, $F^{\text{D}_2\text{O}}$.¹²⁻¹³

$$\%E_{\text{corrected}}^{\text{peptide}}(t_{\text{HDX}}) = \frac{D^{\text{peptide}}(t_{\text{HDX}}) \cdot 100 \%}{F^{\text{D}_2\text{O}}(\langle m(\infty) \rangle^{\text{peptide}} - \langle m(0) \rangle^{\text{peptide}})} \quad (\text{S5})$$

where $\langle m(\infty) \rangle^{\text{peptide}}$ is the centroid mass of a peptide from a protein sample containing only deuterons at its amide sites. Measurements of the control sample, Fab- D_2O , yields $\langle m(\infty_{\text{pseudo}}) \rangle^{\text{peptide}}$, which is conjectured to equal $\langle m(\infty) \rangle^{\text{peptide}}$. The masses $\langle m(t_{\text{HDX}}) \rangle^{\text{peptide}}$ and $\langle m(\infty_{\text{pseudo}}) \rangle^{\text{peptide}}$ are measured using the same apparatus and procedures.

As originally conceived, equation S5 was designed to apply only to the back-exchange of polyalanine peptides for a single-step process. Zhang and Smith simulated the single-step, back-exchange process explicitly for 3000 peptides containing random amino acid sequences containing 5 to 25 amide hydrogens.¹² They found that corrections to the simulations using equation S5 yielded an average error of $(5.5 \pm 5.5) \%$ (1σ). In all, 86 % of peptides had errors of $< 10 \%$.

Software and calculation of uncertainty. All manipulations of spreadsheets reported in CSV format were accomplished with custom programs implemented in Labview 7.1 (National Instruments Corp, Austin, TX). Additional statistical analyses were accomplished using custom scripts implemented in DataPlot.¹⁴⁻¹⁶

In this work some uncertainties are reported as $1s$ and 1σ , where the sample standard deviation is computed by

$$s = \sqrt{\sum_{i=1}^n (x_i - \bar{x})^2 / (n - 1)} \quad (\text{S6})$$

$$\sigma = \sqrt{\sum_{i=1}^n (x_i - \bar{x})^2 / n} \quad (\text{S7})$$

where \bar{x} is the mean of the measurements, x_i are the measured values, and n is the number of measurements. An approximate standard error of the mean is

$$\sigma_{\bar{x}} \approx s / \sqrt{n} \quad (\text{S8})$$

SUPPORTING RESULTS

Intact Mass Spectrometry of Finished Fab-D₂O Samples. Intact mass spectrometry can indicate the existence of amide sites that undergo H/D exchange at extremely slow rates. Intact mass spectrometry measurements on freshly- finished Fab-D₂O control samples were performed on Orbitrap and Q-TOF platforms at NIST. Deconvolution of the $[M+nH]^+$ mass envelopes of the Fab-H₂O sample yielded the molecular mass of $[M] = 47,628 (\pm 2)$ g/mol. Taking into account the N-terminal pyroglutamate residue, this mass is in good accord with the theoretical mass of Fab-H₂O, $[M] = 47,628$ g/mol and a previous measurement of $[M] = 47,628 (\pm 5)$ g/mol with a Q-TOF mass spectrometer.²

Prior to conducting measurements on Fab-D₂O the mass spectrometer sample handling systems were pre-conditioned with 99.96 % D₂O. After conducting measurements by employing the same mass spectrometers and infusion procedures, deconvolution of the $[M+nD]^+$ data for Fab-D₂O yielded the molecular mass of $[M] = 48,206 (\pm 2)$ g/mol. The theoretical mass of Fab-D₂O is 48,390 g/mol.¹⁷ The difference between the measured mass of Fab-D₂O control samples and the theoretical mass indicates that (184 ± 2) protons supplant deuterons in exchangeable sites. These protons may indicate that certain portions of the 412 amide sites of Fab-D₂O are essentially inert to H/D exchange. Alternately, the protons may reside mainly among the 346 amino acid side-group sites that are available to rapid H/D exchange with H₂O within the MS electrospray source. The intact molecule ESI-MS data do not resolve this question of site-occupancy type. This uncertainty of the amide occupancy type within the finished Fab-D₂O control directs us to assume that $\langle m(\infty_{\text{pseudo}}) \rangle^{\text{peptide}} \leq \langle m(\infty) \rangle^{\text{peptide}}$.

Calculation of repeatability, $\langle s^{\text{Lab}} \rangle$. During a run at a laboratory, three reps at each t_{HDX} produce a like number of centroid measurements for each peptide. For each peptide the application of equation S2 produces three $D^{\text{peptide}}(t_{\text{HDX}})$ for three reps. Application of equation S6 to the three $D^{\text{peptide}}(t_{\text{HDX}})$ computes one $s_{\text{peptide}}^{\text{Lab}}(t_{\text{HDX}})$ for the peptide during the run. The $s_{\text{peptide}}^{\text{Lab}}(t_{\text{HDX}})$'s for each peptide are plotted on Figure S7 (blue dots). (For 2 % of all data no $s_{\text{peptide}}^{\text{Lab}}(t_{\text{HDX}})$ is computed because fewer than three $D^{\text{peptide}}(t_{\text{HDX}})$ are available at t_{HDX} for the *peptide*.) This procedure is repeated for the three runs, yielding three $s_{\text{peptide}}^{\text{Lab}}(t_{\text{HDX}})$ for each peptide. The accumulated $s_{\text{peptide}}^{\text{Lab}}$ values across all peptides comprise the repeatability plot for each laboratory. The repeatability plot for each laboratory is constructed from a dataset comprising between 984 to 4057 $s_{\text{peptide}}^{\text{Lab}}$ values for peptides in all reported charge states (Figure S7). At each t_{HDX} the arithmetic mean of $s_{\text{peptide}}^{\text{Lab}}(t_{\text{HDX}})$ across all peptide sequences is computed to find the average repeatability, $\langle s^{\text{Lab}}(t_{\text{HDX}}) \rangle$, which are plotted as red squares on Figure S7. These means are reported in Figure 4. The uncertainty $\langle s^{\text{Lab}} \rangle$ is the standard error of the mean, $\sigma_{\bar{x}}$, which is computed via equation S8.

Using Repeatability plots to assess instrument fitness. A repeatability plot of $s_{\text{peptide}}^{\text{Lab}}$ vs t_{HDX} illuminates on the fitness of the HDX-MS laboratory system and procedures. As examples, the repeatability plots for Lab 1 and Lab 8 (Figures S7A and S7H) exhibit tightly clustered patterns of $\langle s^{\text{Lab } 1} \rangle \leq 0.01$ Da and $\langle s^{\text{Lab } 8} \rangle \leq 0.02$ Da at each t_{HDX} , indicating excellent system fitness.

While a repeatability plot exhibiting a small $\langle s^{\text{Lab}} \rangle$ is a characteristic of good HDX-MS system fitness, the plot can reveal the presence of systemic problems. For example, the repeatability plots for Lab 10 and Lab 12 (Figures S7J and S7L), yield $\langle s^{\text{Lab}} \rangle \approx 0.2$ Da; however, these plots also exhibit outlying

$s_{\text{peptide}}^{\text{Lab}}$ data points that are four to ten times greater than $\langle s^{\text{Lab}} \rangle$ at each t_{HDX} , indicating less than optimal system fitness. The accumulation of numerous large $s_{\text{peptide}}^{\text{Lab}}$ can elevate $\langle s^{\text{Lab}} \rangle$. For example, $\langle s^{\text{Lab } 13} \rangle \approx 0.4$ Da, which is a result of contributions by $s_{\text{peptide}}^{\text{Lab}}$ that are as much as twenty-five times greater than $\langle s^{\text{Lab } 13} \rangle$ (Figure S7M).

The repeatability plot can also reveal procedural problems. For example, Lab 9 (Figure S8I) shows good average repeatability, $\langle s^{\text{Lab } 9} \rangle \leq 0.08$ Da for all t_{HDX} , excepting $t_{\text{HDX}} = 30$ s, where $\langle s^{\text{Lab } 9} \rangle = 0.2$ Da because $s_{\text{peptide}}^{\text{Lab}}$ are dispersed to 1.8 Da. This pattern suggests the possibility of a poorly synchronized robot that is changing the duration of t_{HDX} , such that each rep samples a different $t_{\text{HDX}} \pm \delta$.

Effects of peptide charge on deuterium uptake. For data reported by 13 laboratories the responses of centroids as a function of peptide charge were examined for 513 peptides ($z = +1$ to $+7$) of 107 sequences. (Two laboratories did not report centroid data for multiple charge states.) The centroid data sets were examined for effects due to intermolecular metathesis reactions resulting in H for D exchange. The concern is that reactions in the ESI source may promote H for D exchange in the protic environment of the electrospray ion source, thus, corrupting the nascent deuterium content.¹⁸⁻¹⁹ The rates of such reaction processes are putatively functions of the operating conditions within the ESI source and the peptide reactivity of each charge state.

Since such reaction processes are functions of the peptide physical properties and of the operating conditions within the electrospray ion source, the effects of intramolecular H for D exchange are expected to be prominent for specific ion sequences and specific laboratories. In this view, as z increases for a particular amino acid sequence, the peptides may exhibit decreased centroid mass. Variation of ESI source operating conditions among the laboratories may make this effect prominent in the centroid data reported by one laboratory but absent in others.

To detect the effects of putative intermolecular H/D exchange, the area of each $D^{\text{sequence}}(t_{\text{HDX}})$ vs. $\log_{10}(t_{\text{HDX}})$ plot was integrated over the interval that each peptide is most deuterated, specifically, $t_{\text{HDX}} = (3,600 \text{ s}, 14,400 \text{ s}, \infty_{\text{pseudo}})$. The trapezoidal approximation was used for the integration of each peptide charge state.²⁰⁻²¹ By dividing with a unit area determined by integrating over $\log_{10}(t_{\text{HDX}})$ for $D^{\text{sequence}}(t_{\text{HDX}}) = 1$ and multiplying by 100%, the area is normalized to percent. The calculations yield $\%A_z^{\text{sequence}}(\text{Lab})$, an estimated area of deuterium uptake for a sequence in charge state z . The uncertainty of each $\%A_z^{\text{sequence}}(\text{Lab})$ was computed using the uncertainties of $D^{\text{peptide}}(t_{\text{HDX}})$, which, in turn, are computed from the sample standard deviation of nine centroid measurements at each t_{HDX} . After rejecting outliers residing $\pm 3s$ beyond the mean, the mean uncertainty of $\%A_z^{\text{sequence}}(\text{Lab})$ is $s_z^{\text{sequence area}}$ (equation S7). We adopt the test criteria that $A_z^{\text{sequence}}(\text{Lab})$'s of two charge states of like sequence are unequal when their areas differ by $1s_z^{\text{sequence area}}$, where $s_z^{\text{sequence area}}$ is the larger uncertainty found for each $\%A_z^{\text{sequence}}(\text{Lab})$ pair under comparison. Table S5 lists the reported sequences of $z, z+1, z+2, \dots$ and their relative integrated deuterium content as a function of charge state.

Centroid mass areas derived for 88 % of the 107 peptide sequences fall inside the chosen criterion of $1s_z^{\text{sequence area}}$. The data submitted by the eleven laboratories comprise mainly sequences of $z = +2, +3$ and $z = +3, +4$, but longer series of $z = +1, +2, +3; z = +4, +5, +6$ and $z = +4, +5, +6, +7$ are also present. The $A_z^{\text{sequence}}(\text{Lab})$'s along each series of z differ by $\leq 1s_z^{\text{sequence area}}$ and $1s_{z+n}^{\text{sequence area}}$. Where sequences with charge series of $z = +n, +n+1$, (and occasionally $z = +n+2$) differ by $> 1s_{z+i}^{\text{sequence area}}$ ($i = 0, 1, 2 \dots n$), the lowest charge state, $z = +n$, is twice as likely to manifest the smaller area than the $z = +n+1$ peptide. For the fragments of Fab of NISTmAb the diminished $A_{z+i}^{\text{sequence}}(\text{Lab})$ of the $z = +n$ peptide likely arises from coincidences with eluting LC peaks of similar m/z . Consequently, for this report evaluations of reproducibility have used peptide centroids of the charge state manifesting the least measurement

uncertainty for $A_z^{\text{sequence}}(\text{Lab})$. In short, analyses of peptide centroids in different charge states provides no evidence that systemic, in-ESI source, intermolecular H/D exchange affects data submitted by cohort members.

FIGURES

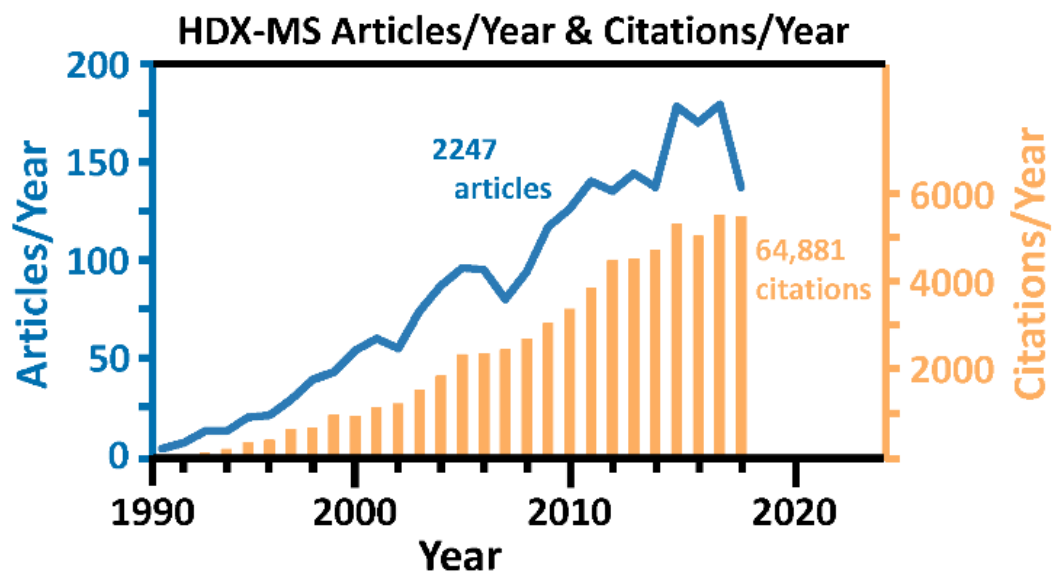


Figure S1. Plot of the number of original research publications (i.e., reviews and commentaries are uncounted) per year that employed hydrogen-deuterium exchange mass spectrometry to investigate protein behavior since its invention in 1991.²²

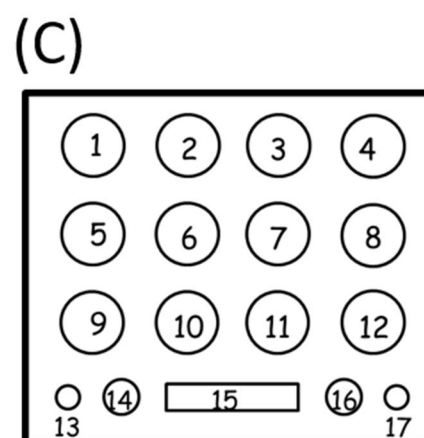
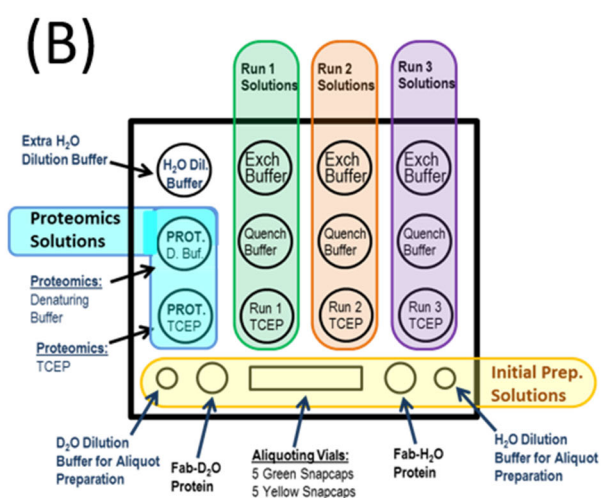
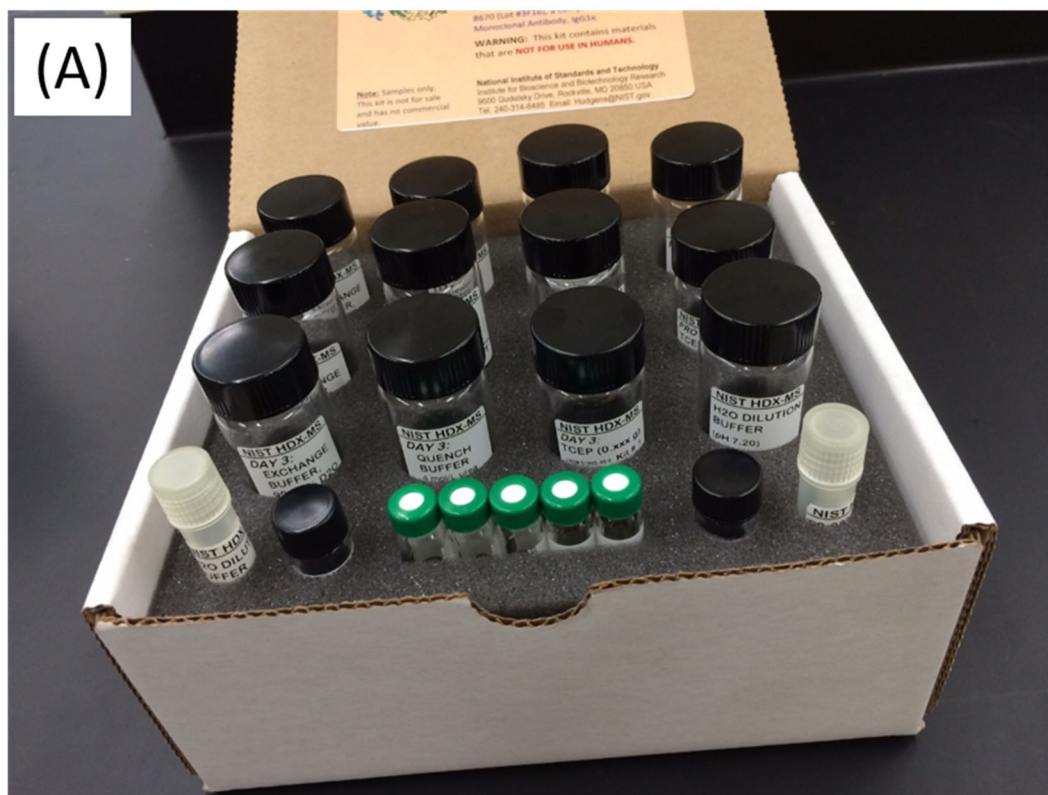


Figure S2. The HDX-MS standard reagent kit. **A)** Kit of reagents and vials. **B)** Location and descriptions of vials inside the kit. Vials are used for the initial preparation of diluted protein aliquots (bottom row), for the development of the proteomics database (leftmost column), and for three HDX-MS experiments (upper right columns). **C)** Map of the vials referenced in Table S1.

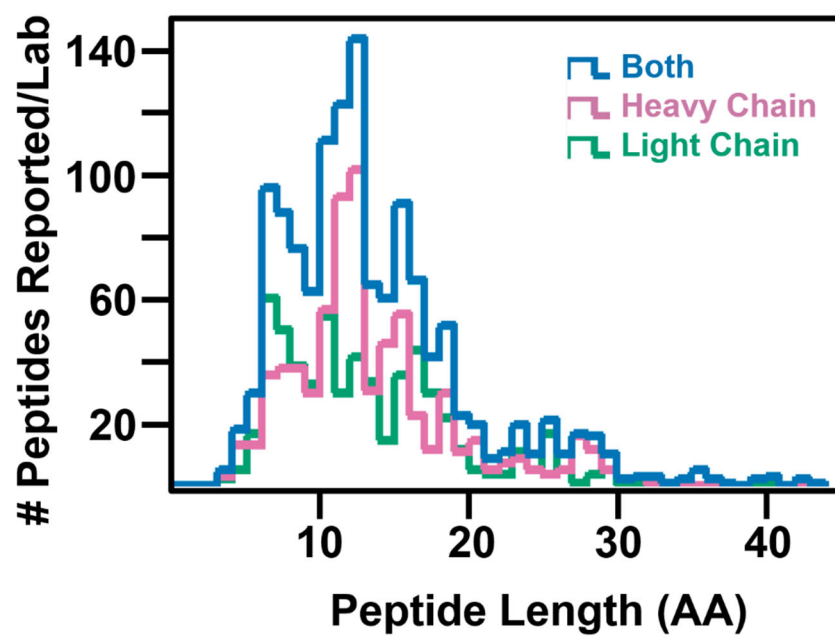


Figure S3. Histogram showing the observation frequency vs peptide amino acid length (AA) for the heavy and light chains of the Fab fragment of NISTmAb after proteolysis in immobilized enzyme columns. (The plot does not show the sparse population of peptide ions near 60 AA.) Fifteen laboratories reported 430 sequences. The median sequence length in this set contains 13 amino acids, and 84 % of the members in the set contain between 5 and 21 amino acids.



Figure S4. Peptide sequences for the heavy chain (HC) and light chain (LC) reported by **A)** Lab 1, **B)** Lab 2, **C)** Lab 3, and **D)** Lab 4. To permit direct comparison of these maps, the *xy*-coordinates of each sequence stripe are the same as in Figure 2 and Figures S4P. Headers note the number of reported sequences and the coverage percentage.

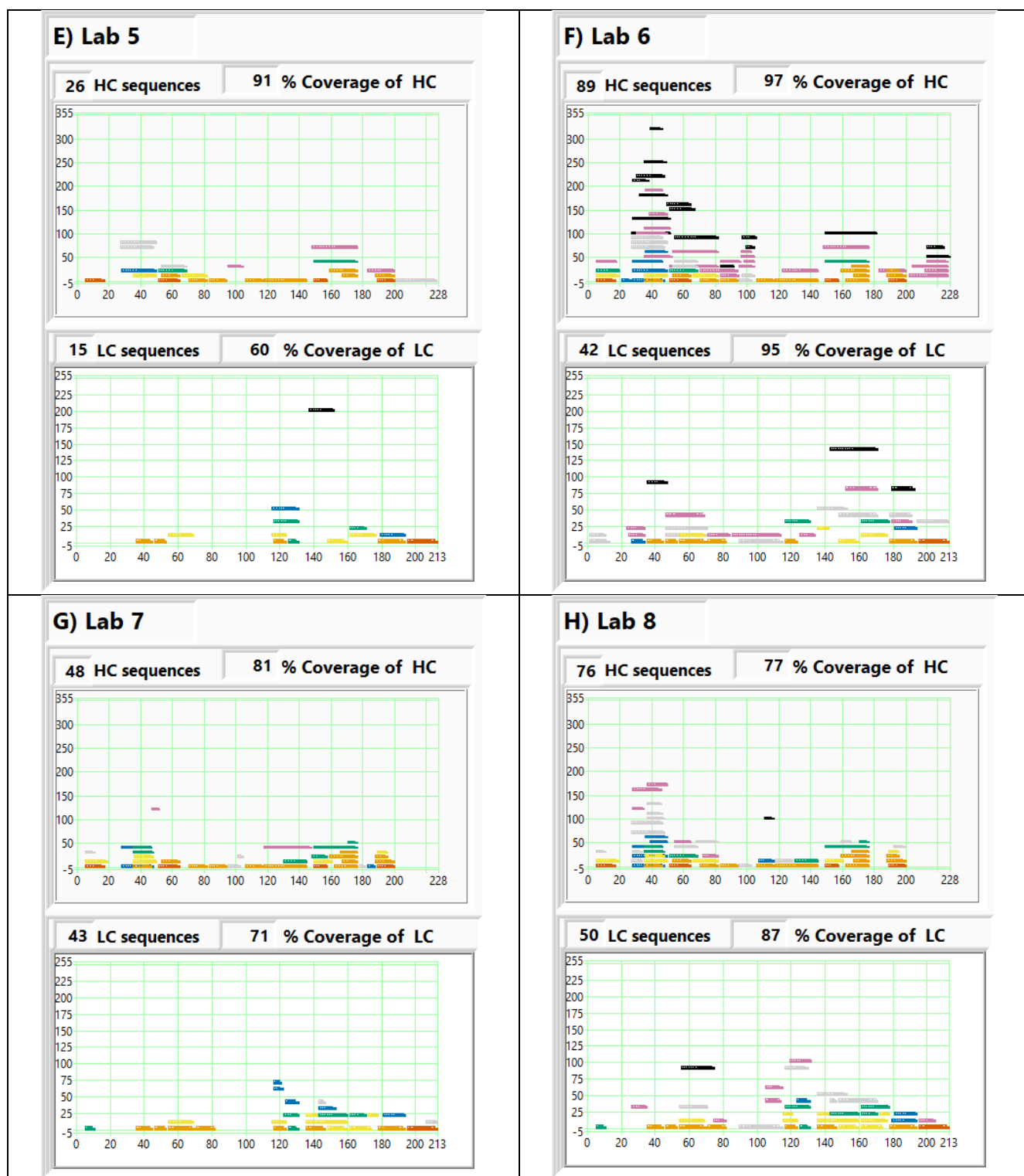


Figure S4 (cont'd). Peptide sequences for the heavy chain (HC) and light chain (LC) reported by **E)** Lab 5, **F)** Lab 6, **G)** Lab 7, and **H)** Lab 8. To permit direct comparison of these maps, the xy -coordinates of each sequence stripe are the same as in Figure 2 and Figures S4P. Headers note the number of reported sequences and the coverage percentage.

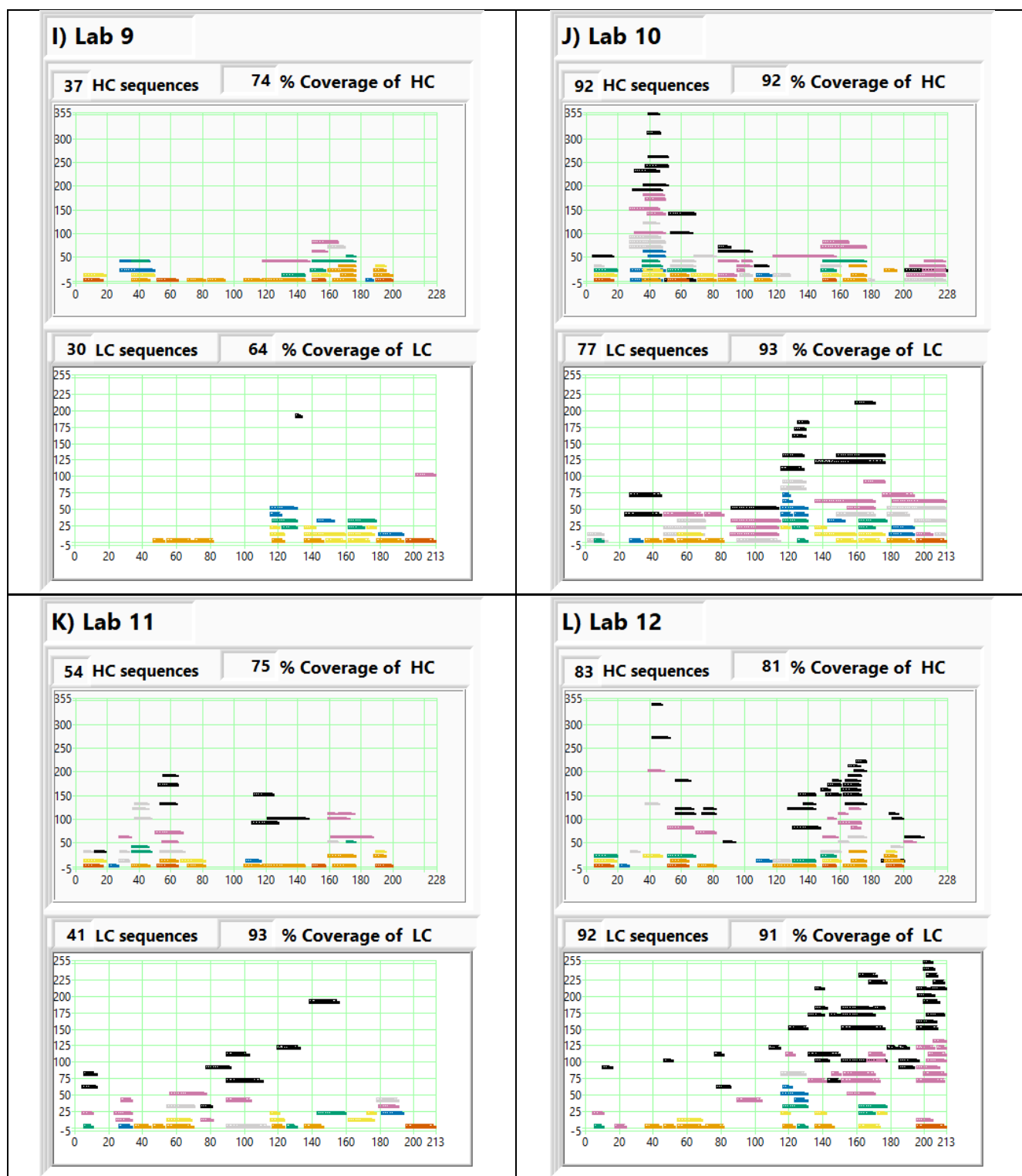


Figure S4 (cont'd). Peptide sequences for the heavy chain (HC) and light chain (LC) reported by **I)** Lab 9, **J)** Lab 10, **K)** Lab 11, and **L)** Lab 12. To permit direct comparison of these maps, the *xy*-coordinates of each sequence stripe are the same as in Figure 2 and Figure S4P. Headers note the number of reported sequences and the coverage percentage.

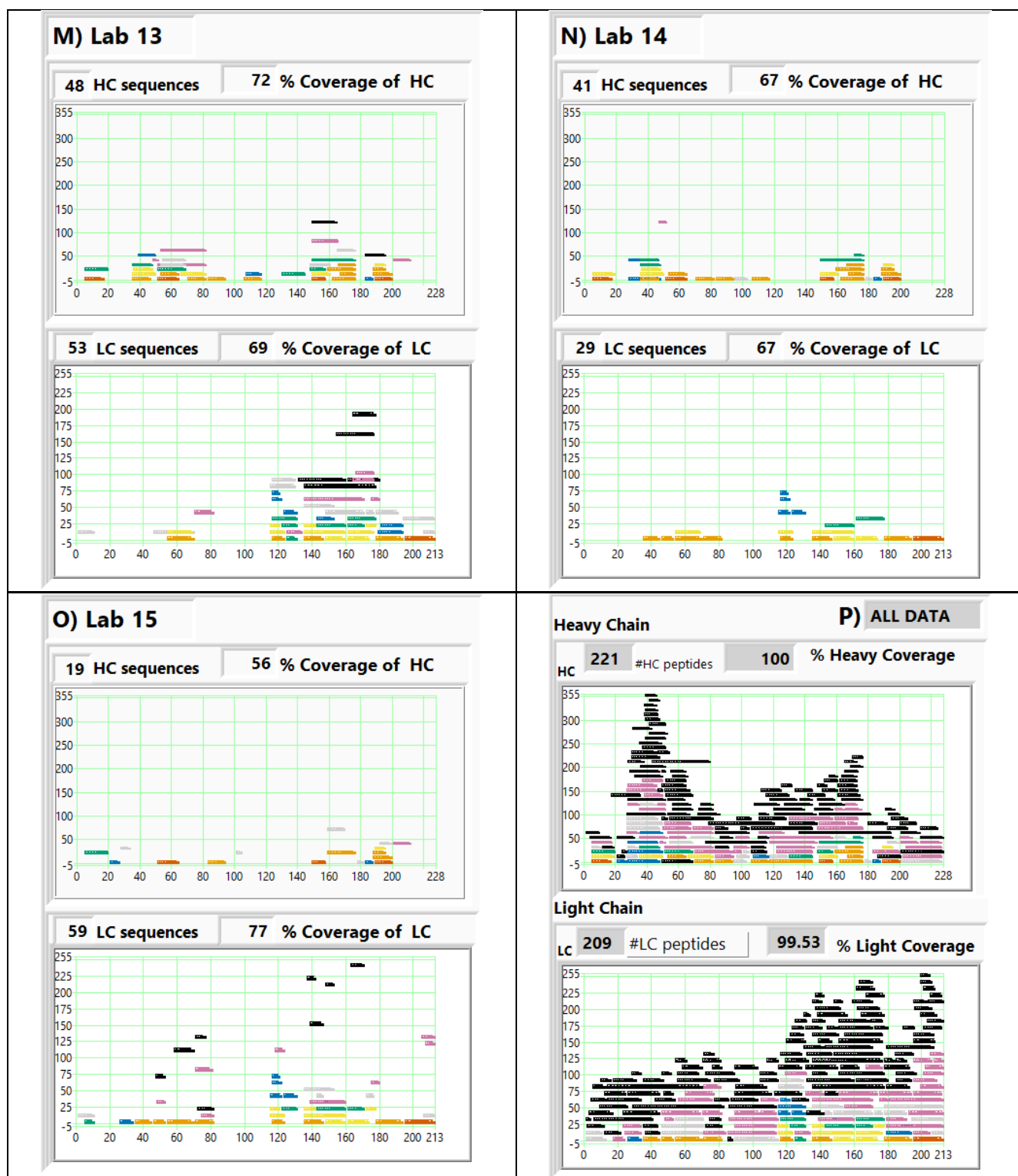


Figure S4 (cont'd). Peptide sequences for the heavy chain (HC) and light chain (LC) reported by **M)** Lab 13, **N)** Lab 14, and **O)** Lab 15. To permit direct comparison of these maps, the *xy*-coordinates of each sequence stripe are the same as in Figure 2 and Figure S4P. **P)** Summary map showing all reported sequences. Headers note the number of reported sequences and the sequence coverage percentage.

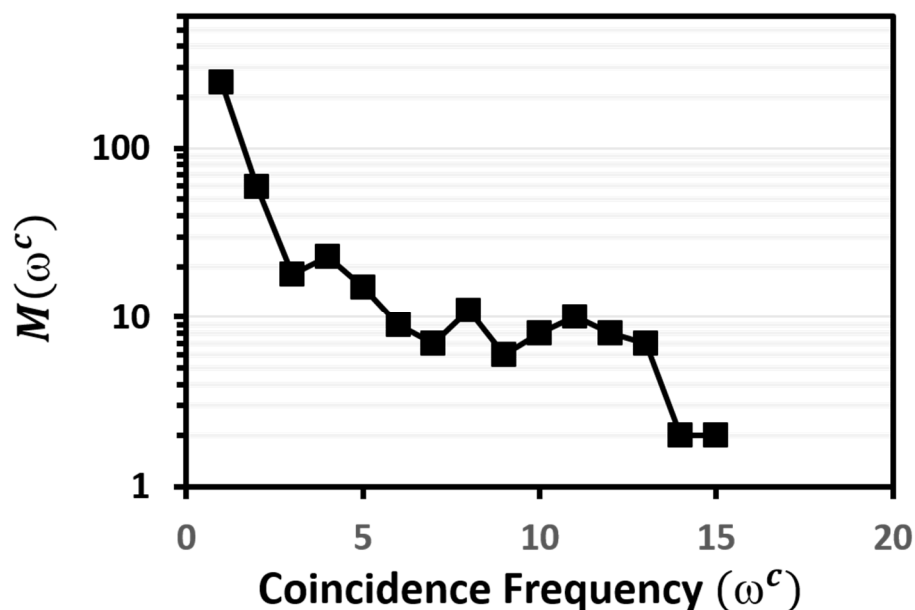


Figure S5. Sequence coincidence population $M(\omega^c)$ vs. Coincidence Frequency (ω^c) for sequences reported by the 15 laboratory cohort. Black squares plot the observed $M(\omega^c)$ found in the cohort data.

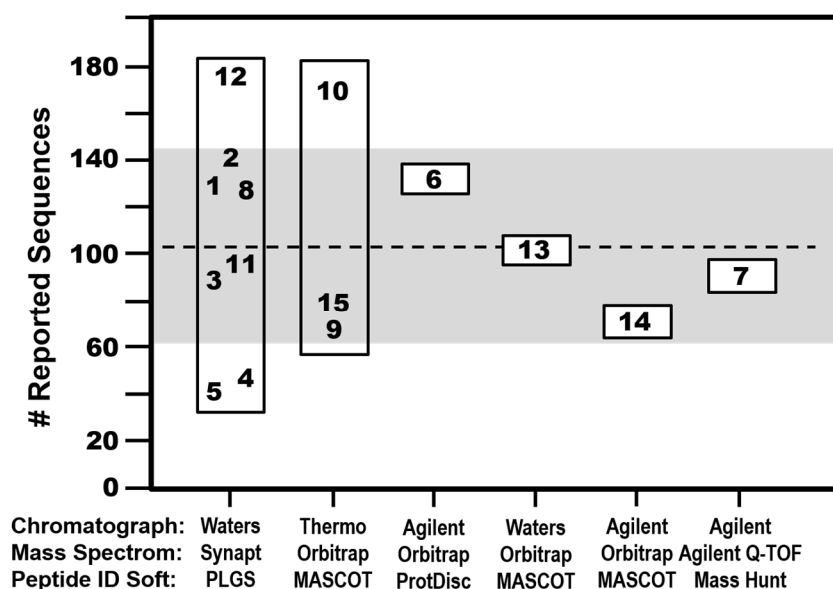


Figure S6. Population of reported peptide sequences as a function of instrument-software configuration. Boxes encompass laboratories (indicated by their numbers) sharing the same instrument-software configuration, and the ordinate of each number denotes number of sequences reported by the laboratory. A dashed line marks $\langle \bar{C} \rangle = 103$, the average number of sequences reported by all laboratories. The shaded area denotes, $\langle \bar{C} \rangle = 103 \pm 41$, the envelop indicating the one standard deviation limit of the sequence populations.

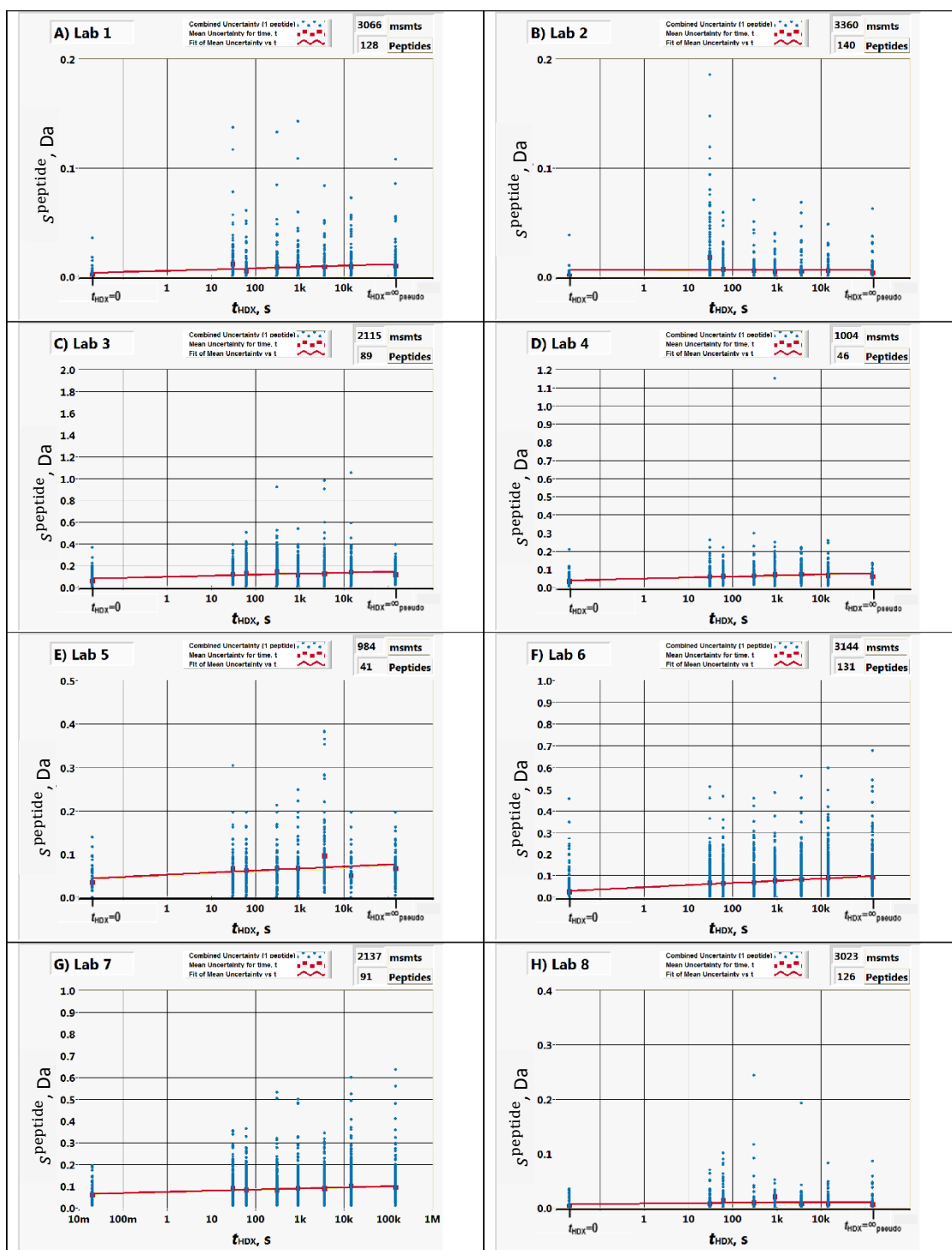


Figure S7. The repeatability plots (s^{peptide} vs t_{HDX}) for: **A)** Lab 1, **B)** Lab 2, **C)** Lab 3, **D)** Lab 4, **E)** Lab 5, **F)** Lab 6, **G)** Lab 7, and **H)** Lab 8. Blue dots mark the $D^{\text{peptide}}(t_{\text{HDX}})$ measurements. Squares mark $\langle s^{\text{Lab}} \rangle$, which is the average of $s^{\text{peptide}}(t_{\text{HDX}})$ for all peptides reported by the indicated laboratory. The red line indicates the fit of $\langle s^{\text{Lab}} \rangle$ vs t_{HDX} . These fits with their uncertainty limits are summarized in Figure 4.

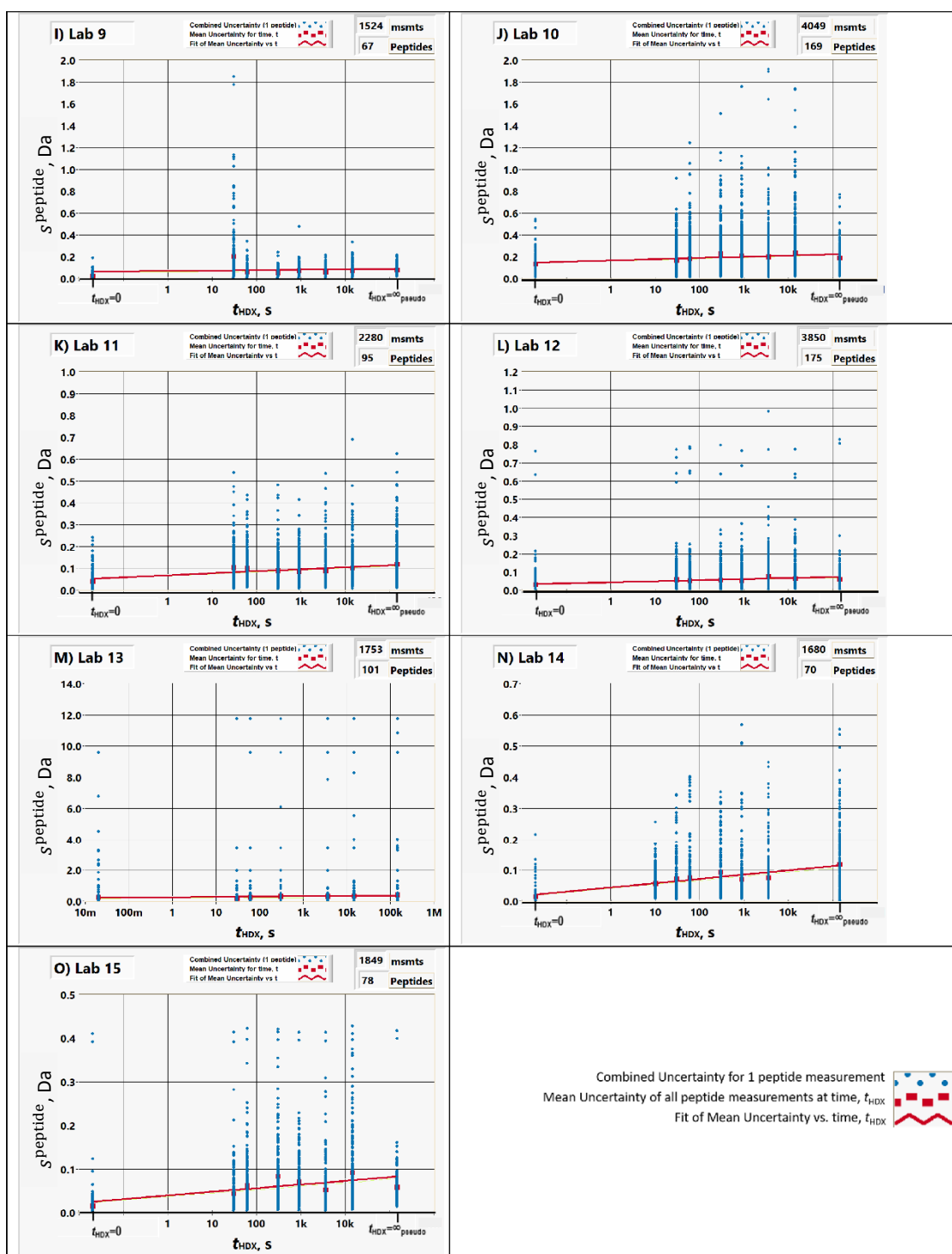


Figure S7 (cont'd). The repeatability plots (s^{peptide} vs t_{HDX}) for: **I)** Lab 9, **J)** Lab 10, **K)** Lab 11, **L)** Lab 12, **M)** Lab 13, **N)** Lab 14, and **O)** Lab 15. Squares mark $\langle s^{\text{Lab}} \rangle$, which is the average of s^{peptide} for all peptides reported by the indicated laboratory at each t_{HDX} . The red line indicates the fit of $\langle s^{\text{Lab}} \rangle$ vs t_{HDX} . These fits with their uncertainty limits are summarized in Figure 4.

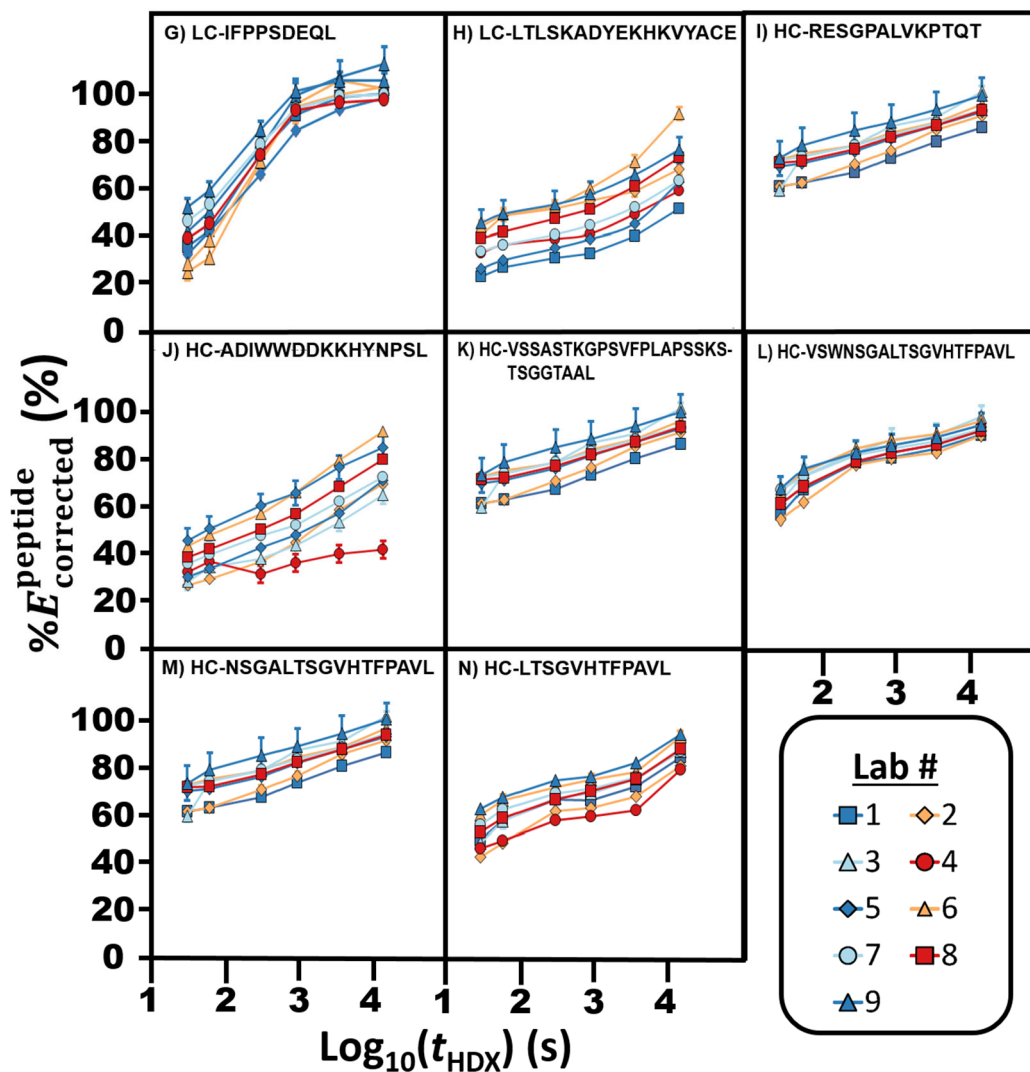


Figure S8. Plots of $\%E^{\text{peptide}}_{\text{corrected}}(t_{\text{HDX}})$ vs $\log_{10}(t_{\text{HDX}})$ for peptides measured at $T_{\text{HDX}} = (25 \pm 1) ^\circ\text{C}$: **G)** LC-¹¹⁶IFPPSDEQL¹²⁴, **H)** LC-¹⁷⁸LTLSKADYKHKVYACE¹⁹⁴, **I)** HC-⁵RESGPALVKPTQT¹⁷, **J)** HC-⁵¹ADIWWDDKKHYNPSL⁶⁵, **K)** HC-¹¹⁸VSSASTKGPSVFPLAPSSKSTSGGTAAL¹⁴⁵, **L)** HC-¹⁵⁹VSWNSGALTSGVHTFPAVL¹⁷⁷, **M)** HC-¹⁶²NSGALTSGVHTFPAVL¹⁷⁷ and **N)** HC-¹⁶⁶LTSGVHTFPAVL¹⁷⁷, Legend indicates the reporting laboratory. Bars indicate uncertainties (1σ) larger than symbols. The letter designation of each panel corresponds to the Peptide list legend of Figure 6A.

TABLES

Table S1. Positions, vial labeling, and chemical information for each vial in the HDX-MS kit.

Vial #	Vial Label	Chemical Contents	Notes
1	Dilution Buffer (H ₂ O, pH 7.4)	20 mmol/L phosphate buffer, 150 mmol/L NaCl in H ₂ O	Measured pH 7.50 (\pm 0.02) VOLUME: 4 mL
2, 3, 4	HDX-Day #: Exchange Buffer 99.98% D ₂ O	20 mmol/L phosphate buffer, 150 mmol/L NaCl in 99.98% D ₂ O	Corrected $pD_{corrected}$ 7.48 (\pm 0.02) VOLUME: 4 mL
5	Proteomics: Quench Buffer	8 mol/L GdnHCl in 0.4 mol/L phosphate	Measured pH 3.1 (\pm 0.02) to be diluted on day of use VOLUME: 4 mL
6, 7, 8	HDX-Day #: Quench Buffer	8 mol/L GdnHCl , 0.4 mol/L phosphate buffer	Measured pH 3.1 (\pm 0.02) VOLUME: 4 mL
9	Proteomics: TCEP-HCl	0.65 – 0.70 g tris (2-carboxyethyl) phosphine hydrochloride	Material must be weighed and added to dilute Quench Buffer (position 5) on day of use.
10, 11, 12	HDX-Day #: TCEP-HCl	0.65 – 0.70 g tris(2-carboxyethyl) phosphine hydrochloride	Material must be weighed and added to dilute Quench Buffer on day of use (See page 9).
13	Dilution Buffer 99.98% D ₂ O	20 mmol/L phosphate buffer, with 150 mmol/L NaCl in 99.98% D ₂ O (4 mL per glass vial and 2.5 mL per plastic vial)	$pD_{corrected}$ 7.48 (\pm 0.02) VOLUME: 2.5 mL
14	Fab-D ₂ O	110 μ mol/L NIST-Fab in 20 mmol/L phosphate buffer, pH 7.5 with 150 mmol/L NaCl in D ₂ O (200 μ L/vial)	200 μ L/vial, spin down contents before use (p. 1) $pD_{corrected}$ 7.48 (\pm 0.02) Prepared on 6 NOV 2014 by resuspension of lyophilized Fab in 99.98 % D ₂ O.
15	Microliter Freezer Vials for aliquoting diluted protein samples	Empty.	5 vials with yellow caps 5 vials with green caps
16	Fab-H ₂ O	200 μ mol/L NIST-Fab in 20 mmol/L phosphate buffer, 150 mmol/L NaCl in H ₂ O buffer	200 μ L/vial, spin down contents before use (p. 1) pH ~ 7.4
17	Dilution Buffer (H ₂ O, pH 7.4)	20 mmol/L phosphate buffer, pH 7.5 with 150 mmol/L NaCl in H ₂ O	Measured pH 7.5 (\pm 0.02) VOLUME: 2.5 mL

Table S2. Instrument-software configurations used by laboratories to analyze and identify peptide ions.

Lab	Sample Handling	Chromatograph	Mass Spectrometer	Peptide ID Software	Centroid software
1	--	Waters ^a	Synapt G2 ^b	PLGS ^c	DynamX 2.0 ^b
2	manual	Waters ^a	Synapt G2 ^b	PLGS ^c	DynamX 3.0 ^b
3	--	Waters ^a	Synapt G2Si ^b	PLGS ^c	DynamX 2.0 ^b
4	robot	Waters ^a	Synapt G2Si ^b	PLGS ^c	DynamX ^b
5	manual	Waters ^a	Synapt G2S ^b	PLGS ^c	DynamX 2.0.0 ^b
6	manual	Agilent ^d	Orbitrap Elite ^e	ProtDisc ^f	DXMS Explorer ^g
7	robot	Agilent ^d	Agilent 6530 Q-TOF ^h	Agilent Mass Hunter Qualitative Analysis ^h	HDEaminer 1.4.0 beta ^g
8	manual	Waters ^a	Synapt G2 ^b	PLGS 3.0 ^c	DynamX 3.0 ^b
9	robot	Thermo ^e	Orbitrap Elite ^e	MASCOT ⁱ	HDX Workbench ^j
10	robot	Thermo ^e	Thermo qExactive Orbitrap ^e	MASCOT ⁱ	HDEaminer ^g
11	manual	Waters ^c	Synapt G2S ^b	PLGS 2.5.2 ^c	DynamX 3.0 ^b
12	robot	Waters ^a	Synapt G2Si ^b	PLGS ^c	DynamX 2.0 ^b
13	robot	Waters ^a	Orbitrap Elite ^e	MASCOT ⁱ	EXMS ^k and in-house developed scripts
14	robot	Agilent ^d	Orbitrap Q-Exactive ^e	MASCOT ⁱ	HDX Workbench ^j
15	robot	Thermo ^e	Orbitrap Elite ^e	MASCOT ⁱ	HDX Workbench ^j

^a) Waters nanoACQUITY UPLC

^b) Waters Corp., Milford, MA

^c) ProteinLynx Global SERVER, Waters Corp., Milford, MA

^d) Agilent 1100 or 1260 series, Agilent Technologies, Inc., Santa Clara, CA

^e) Thermo Fisher Scientific, Santa Clara, CA

^f) Thermo Fisher Proteome Discoverer 1.3, Thermo Fisher Scientific, Santa Clara, CA

^g) Sierra Analytics, Modesto, CA

^h) Agilent Technologies, Inc., Santa Clara, CA

ⁱ) Matrix Science, Oxford, UK

^j) Ref. 9.

^k) Ref. 8.

Table S3. Software search engines and parameters used for identifying the peptide ions, as reported by each laboratory.

Lab	Peptide ID Software	Search against Fab sequence? ^(a)	non-specific enzyme search?	# permitted missed cleavages	Tolerances Precursor & fragment (ppm)	Analysis Mode ^(b)	Minimum Score of accepted peptides	False discovery rate (FDR) (%)	Lock-mass reference reagent ^(c)	Fragment ions per peptide (PLGS only) ^(d)
1	PLGS 2.5.1 ^(e)	Yes	Yes	1	10 / 20	MS ^E	0	4	Leu-Enk	0.3 fragment ions/residue
2	PLGS 2.4 ^(e)	Yes	Yes	1	5 / 20	MS ^E	6.32	4	GluFib	3
3	PLGS 3.0 ^(e)	Yes	Yes	n/a	Automatic	MS ^E	n/a	4 ^(f)	GluFib	≥ 3
4	PLGS 3.0.2 ^(e)	Yes	Yes	1	10 ^(g)	MS ^E	5	4	Lue-Enk	3
5	PLGS 3.0.2 ^(e)	Yes	Yes	3	10 / 10	DDA	10	1	Leu-Enk	n/a
6	ProtDis 1.3 ^(h)	Yes	Yes	2	10 ^(g)	DDA	1.2	0.01		n/a
7	Mass Hunter B.07 ⁽ⁱ⁾	Yes	Yes			DDA		n/a		n/a
8	PLGS 3.0 ^(e)	Yes	Yes		10 ^(g)	MS ^E	ID in 3 out of 4 replicate runs		GluFib	0.2 fragment ions/residue
9	MASCOT 2.3 ^(j)	Yes	Yes	0	20 ^(g)	DDA	20			n/a
10	MASCOT 2.4.1 ^(j)	Yes	Yes		20 ^(g)	DDA	20	n/a		n/a
11	PLGS 2.5.2 ^(e)	Yes	Yes	1	20 ^(g)	MS ^E	n/a	n/a	GluFib	2
12	PLGS ^(e)	Yes	Yes		5, 25	MS ^E	> 7 ^(k)	0	GluFib	0
13	MASCOT 2.3 ^(j)	Yes	Yes	0	10 / (0.8 Da)	DDA	15	n/a		n/a
14	MASCOT 2.1 ^(j)	Yes	Yes	n/a	10 / (15 mDa)	DDA	20		n/a	n/a
15	MASCOT 2.3 ^(j)	Yes	Yes	0	10 / (0.5 Da)	DDA	15	n/a	n/a	n/a

^a Ref. 2.

^b DDA = Data Dependent Acquisition; MS^E = Waters Proprietary method of data acquisition.

^c Leu-Enk: Leucine-Enkephalin (556.2771 Da). GluFib: Glu-Fibrinogen peptide (*m/z* 785.8426).

^d For MS^E data acquisition mode the value specifies the minimum number of observed fragment ions per peptide required to validate the peptide identification.

^e ProteinLynx Global SERVER, Waters Corp., Milford, MA

^f Search against reverse sequence of Fab fragment of NISTmAb.

^g Fragment tolerance not given.

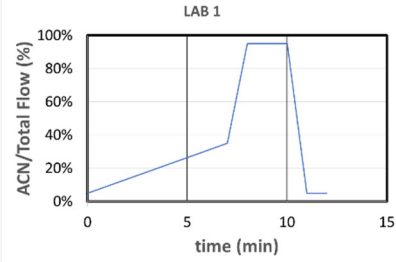
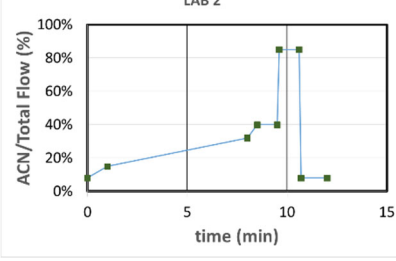
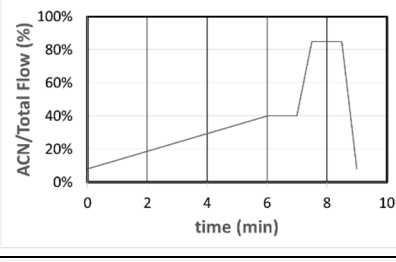
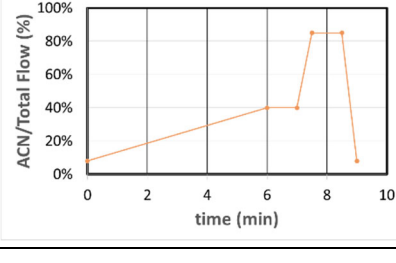
^h Thermo Fisher Scientific, Santa Clara, CA

ⁱ Agilent Mass Hunter Qualitative Analysis B.07, Agilent Technologies, Inc., Santa Clara, CA

^j Matrix Science, Oxford, UK

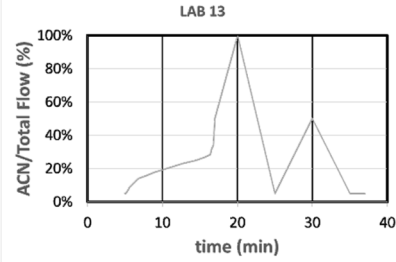
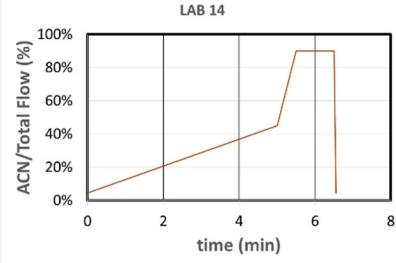
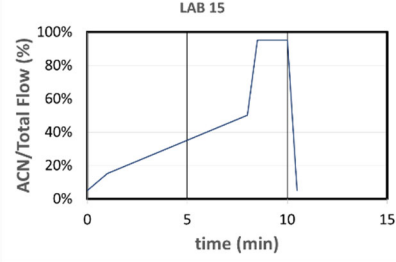
^k Peptide.AutoCurate-Green.

Table S4. Proteolytic and chromatography columns and additional conditions reported by each laboratory.

LAB	Inline Proteolytic column	Trap Column Description	Analytical column	Chromatographic Solvent system	Chromatography Gradient Profile
1	Vendor: Applied Biosystems (Life Technology) Enzyme: Pepsin Poroszyme Immobilized Pepsin Cartridge Dimension (dia. x length, mm): 2.0 X 30	Vendor: Waters Model: VanGard Pre-Column BEH Stationary phase: C18 Dimension (dia. x length, mm): 2.1 x 5	Vendor: Waters Model: Acquity UPLC BEH Stationary phase: C18 Dimension (dia. x length, mm): 2.1 x 100	Solvent A: H ₂ O (0.1% FA) Solvent B: ACN (0.1% FA)	
2	Vendor: Waters Enzyme: Pepsin Model: Enzymate BEH Pepsin Column Dimension (dia. x length, mm): Solvent: H ₂ O + 0.05% TFA @ 75 µL/min	Vendor: Waters Model: ACQUITY UPLC BEH C18 VanGuard Pre-column Stationary phase: C18 Dimension (dia. x length, mm): 2.1 x 5	Vendor: Waters Model: Acquity UPLC BEH Stationary phase: C18 Dimension (dia. x length, mm): 1 x 100	Solvent A: H ₂ O (0.1% FA) Solvent B: ACN (0.1% FA)	
3	Vendor: Waters Enzyme: Pepsin Model: Enzymate BEH Pepsin Column Solvent: 99.9% H ₂ O, 0.1% FA (pH 2.5) @ 100 µL/min	Vendor: Waters Model: ACQUITY UPLC BEH C18 VanGuard Pre-column Stationary phase: C18 Dimension (mm): 2.1 x 5	Vendor: Waters Model: Acquity UPLC BEH Stationary phase: C18 Particle dia. (µm): Dimension (dia. x length, mm): 1 x 100	Solvent A: 99.9% H ₂ O, 0.1% FA, pH 2.5 Solvent B: 99.9% ACN, 0.1% FA, pH 2.5	
4	Vendor: Waters Model: Enzymate Pepsin Column Particle dia.(µm): 5 µm Pore size (Å): 130 Dim. (dia. x length, mm): 2.1 X 30	Vendor: Waters Model: ACQUITY UPLC BEH C18 VanGuard Pre-column, Pore size (Å): 130	Vendor: Waters Model: ACQUITY UPLC BEH Stationary Phase: C18 Particle dia.(µm): 1.7 Dim. (dia. x length, mm): 1 x 100	Solvent A: H ₂ O/0.23% FA Solvent B: ACN/0.23% FA	

LAB	Inline Proteolytic column	Trap Column Description	Analytical column	Chromatographic Solvent system	Chromatography Gradient Profile
5	Vendor: IDEX Model: Guard column Enzyme: Pepsin Functionalization: immobilized pepsin beads (#20343, Thermo) Dimension (dia. x length, mm): 2.0 X 20	Vendor: Waters Model: Acquity BEH Stationary phase: C18 Particle dia. (µm): 1.7 Dimension (dia. x length, mm): 2.1 x 5	Vendor: Waters Model: Acquity UPLC BEH Stationary phase: C18 Particle dia. (µm): 1.7 Dimension (dia. x length, mm): 2.1 x 100	Solvent A: H ₂ O (0.23% FA) Solvent B: ACN (0.23% FA)	
6	Enzyme: Pepsin Linker Chem.: Aldehyde Particle dia.(µm): 20 Dimension (dia. x length, mm): 1 x 20 Solvent: H ₂ O + 0.05% FA @ 20 µL/min	Vendor: Michrom Bioresources Model: Magic C18 Stationary phase: C18 Particle dia. (µm): 3 Dimension (dia. x length, mm): 0.2 x 1.0	Vendor: Michrom Bioresources Model: Magic C18 Stationary phase: C18 Particle dia. (µm): 3 Dimension (dia. x length, mm): 0.2 x 50	Solvent A: H ₂ O, 0.05% TFA Solvent B: 80% ACN, 20% H ₂ O, 0.01% TFA	
7	Vendor: Prepared in lab Enzyme: Pepsin Functionalization: [2] Particle dia.(µm): 20 Dimension (dia. x length, mm): 2.1 x 50	Vendor: Agilent Model: Poroshell 120 EC-C8 Stationary phase: EC-C8 Dimension (dia. x length, mm): 2.1 x 5.0	Vendor: Agilent Model: Zorbax RRHD 300SB-C8 Stationary phase: 300SB-C8 Dimension (dia. x length, mm): 2.1 X 50	Solvent A: 0.1 % FA Solvent B: ACN/H ₂ O/FA (90:10:0.1)	
8	Vendor: AB Porozyme Enzyme: Pepsin Dimension (dia. x length, mm): 2.1 X 30	Vendor: Waters Model: Acquity UPLC BEH VanGuard Stationary phase: C18 Dimension (dia. x length, mm): 2.1 x 5.0	Vendor: Waters Model: Acquity UPLC BEH C18 Stationary phase: C18 Dimension (dia. x length, mm): 2.1 X 100	Solvent A: mqH ₂ O/ 0.23% FA Solvent B: ACN/0.23% FA	

LAB	Inline Proteolytic column	Trap Column Description	Analytical column	Chromatographic Solvent system	Chromatography Gradient Profile
9	Vendor: Waters Enzyme: Pepsin Model: Enzymate BEH Pepsin Column	Vendor: C18 (5 µm) Grace Discovery Sciences, Carnforth, UK Dimension (dia. x length, mm): 1.0 x 50	Vendor: ThermoFisher Scientific (Waltham, MA) Stationary phase: C18 Particle dia. (µm): 1.9 Dimension (dia. x length, mm): 1.0 x 50 mm	Solvent A: H ₂ O + 0.1% FA Solvent B: ACN + 0.1% FA	
10	Enzyme: Pepsin Functionalization: [1] Particle dia.(µm): 20 Dimension (dia. x length, mm): 2.0 x 100 Solvent: H ₂ O + 0.05% TFA @ 500 µL/min	Vendor: Optimize Technologies Model: EXP Stationary phase: Halo Dimension (dia. x length, mm): 2.1 x 5	Vendor: Grace Model: ProZap Expedite MS Stationary phase: C18 Particle dia. (µm): Dimension (dia. x length, mm): 2.1 x 10	Solvent A: H ₂ O + 0.25% FA Solvent B: ACN	
11	Vendor: Applied Biosystems Enzyme: Pepsin Model: Poroszyme Immobilized Pepsin Cartridge Dimension (dia. x length, mm): 2.0 X 30	Vendor: Waters Model: ACQUITY UPLC BEH C18 VanGuard Pre-column Stationary phase: C18 Dimension (dia. x length, mm): 2.1 x 5	Vendor: Waters Model: Acquity UPLC HSS T3 1.8 µm Stationary phase: C18 Particle dia. (µm): 1.8 Dimension (dia. x length, mm): 1 x 50	Solvent A: H ₂ O (0.1% FA) Solvent B: ACN (0.1% FA)	
12	Vendor: NovaBioassay Model: Dual protease column Enzyme: pepsin + Type XIII protease from aspergillus Solvent: H ₂ O with 0.1% FA/8 mM TCEP-HCl @ 75 µL/min	Vendor: Waters Model: ACQUITY UPLC BEH C18 VanGuard Pre-column Stationary phase: C18 Dimension (dia. x length, mm): 2.1 x 5	Vendor: Waters Model: Acquity UPLC BEH Stationary phase: C18 Dimension (dia. x length, mm): 1 x 100	Solvent A: H ₂ O (0.1% FA) Solvent B: ACN (0.1% FA) NOTE: Laboratory changed Quench buffer mixture to: 8 mol/L Urea, 1 mol/L TCEP-HCl, 100 mmol/L PBS adjusted with NaOH to pH 2.5.	

LAB	Inline Proteolytic column	Trap Column Description	Analytical column	Chromatographic Solvent system	Chromatography Gradient Profile
13	Vendor: Life Technology Enzyme: Pepsin Dimension (dia. x length, mm): 2.0 X 30	Vendor: Waters Model: Acquity BEH C18 Vanguard pre-column Stationary phase: C18 Dimension (dia. x length, mm): 2.1 x 5.0	Vendor: Waters Model: Acquity UPLC BEH C18 Stationary phase: C18	Solvent A: 0.1%FA+0.04% TFA in H ₂ O Solvent B: 0.1%FA+0.04% TFA in ACN	
14	Vendor: Waters Enzyme: Pepsin Model: Enzymate BEH Pepsin Column Dimension (dia. x length, mm): Solvent: H ₂ O + 0.1% TFA @ 200 µL/min	Vendor: Waters Model: Symmetry C8 Stationary phase: C18 Dimension (dia. x length, mm): 2.1 x 10	Vendor: ThermoFisher Scientific Model: C18 Hypersil GOLD Stationary phase: Silica based C18 Particle dia. (µm): Dimension (dia. x length, mm): 2.1 x 50 mm	Solvent A: H ₂ O 0.3% FA Solvent B: 90% ACN 10% H ₂ O: 0.3% FA	
15	Vendor: Waters Model: Enzymate BEH Pepsin Column	Vendor: Grace Discovery Sciences (Carnforth, UK) Stationary phase: C18 Particle dia. (µm): 5 Dimension (dia. x length, mm): 1.0 x 50.0	Vendor: ThermoFisher Scientific (Waltham, MA) Model: Hypersil GOLD Stationary phase: C18 Particle dia. (µm): 1.9 Dimension (dia. x length, mm): 1.0 x 50 mm	Solvent A: H ₂ O + 0.1% FA Solvent B: ACN + 0.1% FA	

[1] Refs. 23-24.

[2] Ref. 12.

Table S5. Physio-chem and fluidic conditions reported by each laboratory for HDX-MS measurements.

Lab	T_{HDX} (°C)	Protein Conc during Labeling, $\mu\text{mol/L}$	D_2O Fraction during Labeling, $F^{\text{D}_2\text{O}}$	T_{quench} (°C)	Quench Solution pH	D_2O Fraction during Quench, $F^{\text{D}_2\text{O}}$	Flow Rate through Proteolytic column ($\mu\text{L/min}$)	FROZEN ^(a)	$t_{\text{proteolysis}}$ (s) @ $T_{\text{proteolysis}}$ (s @ °C)	Trap Column Solvent Exchange, (s @ $\mu\text{L/min}$)	T_{LC} (°C)	ESI Source Capillary T (°C)
1	25 ± 0.1	7.5	0.85	0	2.47 to 2.50	0.21	200	No	- - ^(b) @ 10 °C	None	1 ± 0.1	80
2	25	13.3	0.93	0	2.48 to 2.51	0.47	75	No	240 s @ 20 °C	None	0	175
3	25 ± 0.1	8.0	0.84	1 ± 0.5	2.49 to 2.50	0.42	100	No	180 s @ 1 °C	180 s @ 100	3 ± 0.02	80
4	25 ± 0.1	4.16	0.92	2.5 ± 0.1	2.46 to 2.54	0.46	100	No	180 s @ 20 °C	180 s @ 100	0 ± 0.1	175
5	24 ± 0.1	0.43	0.90	0 ± 1	2.44 to 2.55	0.45	300	Yes	120 s @ 18 °C	120 s @ 300	0 ± 0.5	80
6	25.4 ± 0.1	16.7	0.83	1.5 ± 0.1	2.5	0.33	20	Yes	48 s @ 1.5 °C	none	1.5 ± 0.1	200
7	25 ± 0.1	1.2	0.95	1 ± 0.3	2.47 to 2.49	0.48	200	No	180 s @ 0 °C	60 s @ 200	0 ± 0.2	325
8	25 ± 0.1	2.0	0.96	0 ± 0.5	2.49 to 2.5	0.48	150	Yes	18 s @ 20 °C	180 s @ 40	0 ± 1	90
9	25 ± 0.1	0.56	0.86	1 ± 0.1	2.5	0.43	50	No	130 s @ 8 °C	50 s @ 30	1.5 ± 0.1	240
10	20 ± 1	4.55	0.91	0 ± 1	2.5	0.18	500	Yes	30 s @ 3 °C	none	0 ± 1	225
11	20 ± 1	2.0	0.90	20 ± 1	2.51 to 2.52	0.45	100	Yes	180 s @ 15 °C	none	0 ± 0.5	150
12	22 ± 1	2.83	0.94	4	2.51 to 2.52	0.47	75	No	150 s @ 15 °C ^(c,d)	none	0 ± 0.1	80
13	22 ± 0.5	2.99	0.94	0 ± 0.5	2.54 to 2.57	0.47	100	No	130 s @ 0 °C	100 @ 100	0 ± 0.5	250
14	3.6 ± 0.2	10.0	0.80	1.8 ± 0.1	2.46 to 2.47	0.40		No	150 s @ 15 °C	none	3.6 ± 0.2	320
15	3.6 ± 0.1	0.56	0.86	1.0 ± 0.1	2.5	0.43	50	No	180 s @ 8 °C	180 @ 50	1.5 ± 0.1	240

a) FROZEN = “Yes” when sample was frozen at -80 °C immediately after Quench Step (ref. Figure 1B).

b) Value is not reported.

c) Proteolysis column contained pepsin and Type XIII protease from aspergillus.

d) The laboratory used 8 mol/L urea in place of guanidinium chloride.

Table S6. Table of relative $A_z^{\text{total}} = \int \%D_z^{\text{peptide}}(t_{\text{HDX}})d\log_{10}(t_{\text{HDX}})$ integrated over $t_{\text{HDX}} = (3,600 \text{ s}, 14,400 \text{ s}, \infty_{\text{pseudo}})$. For each sequence cells colored blue exhibited the greatest integrated deuterium content, A_z^{total} , and cells colored red have A_z^{total} that are depressed by at least 1s relative to the blue cells.

LEGEND:

	Areas are essentially equal: $A_z^{\text{total}} \pm s \approx A_{z+i}^{\text{total}} \pm s$
	Area of A_z^{total} and A_{z+i}^{total} do not match: $A_z^{\text{total}} \pm s < A_{z+i}^{\text{total}} \pm s$

z= +7	z= +6	z= +5	z= +4	z= +3	z= +2	z= +1	LAB	Sequence
							2	HC/5-19
							2	HC/35-47
							2	HC/35-48
							2	HC/36-47
							2	HC/36-48
							2	HC/51-65
							2	HC/51-69
							2	HC/53-65
							2	HC/66-82
							2	HC/68-82
							2	HC/70-82
							2	HC/83-94
							2	HC/106-117
							2	HC/107-117
							2	HC/118-145
							2	HC/118-158
							2	HC/130-158
							2	HC/149-158
							2	HC/159-170
							2	HC/159-177
							2	HC/166-177
							2	HC/167-177
							2	HC/188-200
							2	HC/189-200
							2	LC/35-45
							2	LC/46-53
							2	LC/71-82
							2	LC/115-124
							2	LC/116-124
							2	LC/135-142

z= +7	z= +6	z= +5	z= +4	z= +3	z= +2	z= +1	LAB	Sequence
							2	LC/135-147
							2	LC/135-160
							2	LC/143-160
							2	LC/178-213
							2	LC/179-213
							2	LC/181-213
							2	LC/195-213
							4	HC/111-127
							4	LC/195-213
							5	HC/5-17
							5	HC/83-94
							6	HC/5-19
							6	HC/5-20
							6	HC/28-47
							6	HC/28-50
							6	HC/35-47
							6	HC/35-50
							6	HC/35-53
							6	HC/36-50
							6	HC/51-65
							6	HC/51-69
							6	HC/51-82
							6	HC/53-65
							6	HC/70-94
							6	HC/122-145
							6	HC/-16--1
							6	HC/-26--1
							6	LC/46-70
							6	LC/46-71
							6	LC/178-191
							6	LC/178-194
							6	LC/181-194
							6	LC/194-213
							6	LC/195-213
							7	HC/5-17
							7	HC/5-19
							7	HC/51-65
							7	HC/53-65
							7	HC/70-82
							7	HC/149-177

z= +7	z= +6	z= +5	z= +4	z= +3	z= +2	z= +1	LAB	Sequence
							7	HC/159-177
							7	HC/162-177
							7	HC/188-196
							7	HC/188-200
							7	HC/189-196
							7	HC/189-200
							7	LC/35-45
							7	LC/115-124
							7	LC/116-124
							7	LC/135-160
							7	LC/143-153
							7	LC/148-160
							7	LC/161-171
							7	LC/161-174
							7	LC/172-178
							7	LC/178-194
							7	LC/181-194
							7	LC/195-213
							7	LC/206-213
							8	HC/5-17
							8	HC/5-19
							8	HC/28-48
							8	HC/35-47
							8	HC/35-50
							8	HC/36-50
							8	HC/39-50
							8	HC/51-65
							8	HC/51-69
							8	HC/54-65
							8	HC/66-82
							8	HC/68-82
							8	HC/70-82
							8	HC/83-94
							8	HC/106-117
							8	HC/118-129
							8	HC/118-145
							8	HC/149-158
							8	HC/159-177
							8	HC/188-200
							8	LC/26-35

z= +7	z= +6	z= +5	z= +4	z= +3	z= +2	z= +1	LAB	Sequence
							8	LC/35-45
							8	LC/115-124
							8	LC/135-153
							8	LC/135-160
							8	LC/178-194
							8	LC/195-213
							9	HC/5-19
							9	HC/35-50
							9	HC/51-65
							9	HC/106-117
							9	HC/149-158
							9	HC/159-177
							9	LC/115-124
							9	LC/135-142
							9	LC/179-194
							9	LC/195-213
							10	HC/5-17
							10	HC/5-19
							10	HC/5-20
							10	HC/35-50
							10	HC/36-48
							10	HC/36-50
							10	HC/51-65
							10	HC/51-69
							10	HC/53-65
							10	HC/53-69
							10	HC/54-69
							10	HC/66-82
							10	HC/68-82
							10	HC/83-94
							10	HC/149-177
							10	HC/-15--1
							10	HC/-27--1
							10	LC/46-53
							10	LC/46-69
							10	LC/46-70
							10	LC/135-142
							10	LC/135-160
							10	LC/175-194
							10	LC/178-194

z= +7	z= +6	z= +5	z= +4	z= +3	z= +2	z= +1	LAB	Sequence
							10	LC/179-194
							10	LC/181-194
							10	LC/181-213
							10	LC/194-213
							10	LC/195-213
							11	HC/5-17
							11	HC/5-17
							11	HC/5-19
							11	HC/5-19
							11	HC/35-47
							11	HC/35-47
							11	HC/35-48
							11	HC/36-46
							11	HC/50-68
							11	HC/50-68
							11	HC/51-65
							11	HC/51-65
							11	HC/53-65
							11	HC/53-65
							11	HC/66-82
							11	HC/66-82
							11	HC/70-82
							11	HC/118-145
							11	HC/161-188
							11	LC/27-34
							11	LC/35-45
							11	LC/54-69
							11	LC/54-70
							11	LC/56-78
							11	LC/135-147
							12	HC/5-20
							12	HC/39-49
							12	HC/51-65
							12	HC/51-68
							12	HC/51-69
							12	HC/69-82
							12	HC/70-82
							12	HC/107-117
							12	HC/159-166
							12	HC/159-174

z= +7	z= +6	z= +5	z= +4	z= +3	z= +2	z= +1	LAB	Sequence
							12	HC/166-173
							12	HC/167-173
							12	HC/200-208
							12	LC/118-124
							12	LC/123-131
							12	LC/135-147
							12	LC/145-151
							12	LC/151-174
							12	LC/161-174
							12	LC/161-178
							12	LC/167-177
							12	LC/195-206
							12	LC/195-209
							12	LC/195-212
							12	LC/195-213
							12	LC/199-213
							12	LC/202-213
							13	HC/35-50
							13	HC/51-65
							13	HC/53-65
							13	HC/66-82
							13	HC/70-82
							13	HC/149-158
							13	HC/188-200
							13	HC/189-200
							13	LC/115-124
							13	LC/116-124
							13	LC/135-153
							13	LC/135-160
							13	LC/143-160
							13	LC/178-194
							14	HC/5-17
							14	HC/35-46
							14	HC/35-47
							14	HC/35-50
							14	HC/36-48
							14	HC/51-65
							14	HC/53-65
							14	HC/70-82
							14	HC/83-94

z= +7	z= +6	z= +5	z= +4	z= +3	z= +2	z= +1	LAB	Sequence
							14	HC/106-117
							14	HC/188-200
							14	LC/35-45
							14	LC/46-53
							14	LC/71-82
							14	LC/115-124
							14	LC/116-124
							14	LC/135-147
							14	LC/135-160
							14	LC/143-160
							14	LC/195-213
							15	HC/83-94
							15	HC/188-200
							15	LC/46-53
							15	LC/54-70
							15	LC/71-82
							15	LC/116-124
							15	LC/135-142
							15	LC/135-147
							15	LC/135-160
							15	LC/139-160
							15	LC/143-160
							15	LC/148-160
							15	LC/161-174
							15	LC/195-213

REFERENCES

1. Marino, J. P.; Brinson, R. G.; Hudgens, J. W.; Ladner, J. E.; Gallagher, D. T.; Gallagher, E. S.; Arbogast, L. W.; Huang, R. Y. C., Emerging Technologies To Assess the Higher Order Structure of Monoclonal Antibodies. In *State-of-the-Art and Emerging Technologies for Therapeutic Monoclonal Antibody Characterization, Vol 3: Defining the Next Generation of Analytical and Biophysical Techniques*, Schiel, J. E.; Davis, D. L.; Borisov, O. V., Eds. 2015; Vol. 1202, pp 17-43.
2. Karageorgos, I.; Gallagher, E. S.; Galvin, C.; Gallagher, D. T.; Hudgens, J. W., Biophysical characterization and structure of the Fab fragment from the NIST reference antibody, RM 8671. *Biologicals* **2017**, *50*, 27-34.
3. Gallagher, D. T.; Karageorgos, I.; Hudgens, J. W.; Galvin, C. V., Data on crystal organization in the structure of the Fab fragment from the NIST reference antibody, RM 8671. *Data in Brief* **2018**, *16*, 29-36.

4. Glasoe, P. K.; Long, F. A., Use Of Glass Electrodes To Measure Acidities In Deuterium Oxide. *The Journal of Physical Chemistry* **1960**, *64* (1), 188-190.
5. Brinson, R. G.; Marino, J. P.; Delaglio, F.; Arbogast, L. W.; Evans, R. M.; Kearsley, A.; Gingras, G.; Ghasriani, H.; Aubin, Y.; Pierens, G. K.; Jia, X. Y.; Mobli, M.; Grant, H. G.; Keizer, D. W.; Schweimer, K.; Stahle, J.; Widmalm, G.; Zartler, E. R.; Lawrence, C. W.; Reardon, P. N.; Cort, J. R.; Xu, P.; Ni, F.; Yanaka, S.; Kato, K.; Parnham, S. R.; Tsao, D.; Blomgren, A.; Rundlof, T.; Trieloff, N.; Schmieder, P.; Ross, A.; Skidmore, K.; Chen, K.; Keire, D.; Freedberg, D. I.; Suter-Stahel, T.; Wider, G.; Ilc, G.; Plavec, J.; Bradley, S. A.; Baldisseri, D. M.; Sforca, M. L.; Zeri, A. C. D.; Wei, J. Y.; Szabo, C. M.; Amezcua, C. A.; Jordan, J. B.; Wikstrom, M., Enabling adoption of 2D-NMR for the higher order structure assessment of monoclonal antibody therapeutics. *Mabs* **2019**, *11* (1), 94-105.
6. Zhang, Z.; Marshall, A. G., A universal algorithm for fast and automated charge state deconvolution of electrospray mass-to-charge ratio spectra. *J. Am. Soc. Mass Spectrom.* **1998**, *9* (3), 225-233.
7. Weis, D. D., *Hydrogen Exchange Mass Spectrometry of Proteins: Fundamentals, Methods, and Applications*. 1st Ed. ed.; John Wiley & Sons, Ltd.: Chichester, 2016.
8. Kan, Z.-Y.; Mayne, L.; Chetty, P. S.; Englander, S. W., ExMS: Data Analysis for HX-MS Experiments. *J. Am. Soc. Mass Spectrom.* **2011**, *22*, 1906-1915.
9. Pascal, B. D.; Willis, S.; Lauer, J. L.; Landgraf, R. R.; West, G. M.; Marciano, D.; Novick, S.; Goswami, D.; Chalmers, M. J.; Griffin, P. R., HDX Workbench: Software for the Analysis of H/D Exchange MS Data. *J. Am. Soc. Mass Spectrom.* **2012**, *23* (9), 1512-1521.
10. Bai, Y. W.; Milne, J. S.; Mayne, L.; Englander, S. W., Primary Structure Effects on Peptide Group Hydrogen-Exchange. *Proteins-Structure Function and Genetics* **1993**, *17* (1), 75-86.
11. Engen, J. R.; Wales, T. E., Analytical Aspects of Hydrogen Exchange Mass Spectrometry. In *Annual Review of Analytical Chemistry, Vol 8*, Cooks, R. G.; Pemberton, J. E., Eds. Annual Reviews: Palo Alto, 2015; Vol. 8, pp 127-148.
12. Zhang, Z.; Smith, D. L., Determination of amide hydrogen exchange by mass spectrometry: A new tool for protein structure elucidation. *Protein Science* **1993**, *2*, 522-531.
13. Mayne, L., Chapter Thirteen - Hydrogen Exchange Mass Spectrometry. In *Methods in Enzymology*, Kelman, Z., Ed. Academic Press: 2016; Vol. 566, pp 335-356.
14. Filliben, J. J.; Tobias, P.; Trutna, L., Design of Experiments (DOE) Mean Plot. In *NIST/SEMATECH e-Handbook of Statistical Methods*, National Institute of Standards and Technology: 2003.
15. Filliben, J. J., "DATAPLOT—Introduction and Overview", NIST Special Publication 667 pdf version. National Bureau of Standards: Gaithersburg, MD, 1984.
<http://www.itl.nist.gov/div898/software/dataplot/sp667.pdf>.
16. Heckert, N. A.; Filliben, J. J. Dataplot. <http://www.itl.nist.gov/div898/software/dataplot/> (accessed 4 OCT 2017).
17. Kavan, D.; Man, P. MSTools - Web based application for visualization and presentation of HXMS data *Int. J. Mass Spectrom.* [Online], 2011, p. 53-58.
<http://www.hxms.com/mstools/HDExCalc/HDExCalc.php> (accessed 7/1/2018).
18. Yury, K.; Alexey, K.; Igor, P.; Eugene, N., Conformational changes of ubiquitin during electrospray ionization as determined by in-ESI source H/D exchange combined with high-resolution MS and ECD fragmentation. *Journal of Mass Spectrometry* **2014**, *49* (10), 989-994.
19. Kim, H. J.; Liyanage, O. T.; Mulenios, M. R.; Gallagher, E. S., Mass Spectral Detection of Forward- and Reverse-Hydrogen/Deuterium Exchange Resulting from Residual Solvent Vapors in Electrospray Sources. *J. Am. Soc. Mass Spectrom.* **2018**.

20. Mazur, S. J.; Gallagher, E. S.; Debnath, S.; Durell, S. R.; Anderson, K. W.; Jenkins, L. M. M.; Appella, E.; Hudgens, J. W., Conformational Changes in Active and Inactive States of Human PP2C alpha Characterized by Hydrogen/Deuterium Exchange-Mass Spectrometry. *Biochemistry* **2017**, *56* (21), 2676-2689.
21. Mazur, S. J.; Weber, D. P., The Area Between Exchange Curves as a Measure of Conformational Differences in Hydrogen-Deuterium Exchange Mass Spectrometry Studies. *J. Am. Soc. Mass Spectrom.* **2017**, *28* (5), 978-981.
22. Web of Science Database Search on HDX-MS of proteins and peptides (no reviews or commentary). Clarivate Analytics: Philadelphia, PA, 2019; (accessed 18 FEB 2019).
23. Wang, L.; Pan, H.; Smith, D. L., Hydrogen Exchange-Mass Spectrometry: Optimization of Digestion Conditions. *Mol. Cell. Proteomics* **2002**, *1* (2), 132-138.
24. Busby, S. A.; Chalmers, M. J.; Griffin, P. R., Improving digestion efficiency under H/D exchange conditions with activated pepsinogen coupled columns. *International Journal of Mass Spectrometry* **2007**, *259* (1), 130-139.